[36] Hämäläinen A, Tervo S, Grau-Olivares M, Niskanen E, Pennanen C, Huuskonen J, et al. Voxel-based morphometry to detect brain atrophy in progressive mild cognitive impairment. Neuroimage 2007;37:1122–31.
[37] Karas G, Sluimer J, Goekoop R, van der Flier W, Rombouts SA, Vrenken H, et al. Amnestic mild cognitive impairment: structural MR imaging findings predictive of conversion to Alzheimer disease. Am J Neuroradiol 2008;29:944–9.
[38] Jack Jr CR, Lowe VJ, Senjem ML, Weigand SD, Kemp BJ, Shiung MM, et al. ^{11}C PiB and structural MRI provide complementary information in imaging of Alzheimer's disease and amnestic mild cognitive impairment. Brain 2008;131:665–80.
[39] McKhann G, Drachman D, Folstein M, Katzman R, Price D, Stadlan EM. Clinical diagnosis of Alzheimer's disease: report of the NINCDS-ADRDA Work Group under the auspices of Department of Health and Human Services Task Force on Alzheimer's Disease. Neurology 1984;34:939–44.
[40] Petersen RC, Smith GE, Waring SC, Ivnik RJ, Tangalos EG, Kokmen E. Mild cognitive impairment: clinical characterization and outcome. Arch Neurol 1999;56:303–8.
[41] Ashburner J, Friston KJ. Voxel-based morphometry—the methods. Neuroimage 2000;11:805–21.
[42] Hirata Y, Matsuda H, Nemoto K, Ohnishi T, Hirao K, Yamashita F, et al. Voxel-based morphometry to discriminate early Alzheimer's disease from controls. Neurosci Lett 2005;382:269–74.
[43] Pike KE, Savage G, Villemagne VL, Ng S, Moss SA, Maruff P, et al. Beta-amyloid imaging and memory in non-demented individuals: evidence for preclinical Alzheimer's disease. Brain 2007;130:2837–44.
[44] Engler H, Forsberg A, Almkvist O, Blomquist G, Larsson E, Savitcheva I, et al. Two-year follow-up of amyloid deposition in patients with Alzheimer's disease. Brain 2006;129:2856–66.
[45] Archer HA, Edison P, Brooks DJ, Barnes J, Frost C, Yeatman T, et al. Amyloid load and cerebral atrophy in Alzheimer's disease: an ^{11}C-PIB positron emission tomography study. Ann Neurol 2006;60:145–7.
[46] Josephs KA, Whitwell JL, Ahmed Z, Shiung MM, Weigand SD, Knopman DS, et al. Beta-amyloid burden is not associated with rates of brain atrophy. Ann Neurol 2008;63:204–12.

Journal of Neurochemistry JNC

JOURNAL OF NEUROCHEMISTRY | 2009 | 109 | 1648–1657 doi: 10.1111/j.1471-4159.2009.06069.x

A traditional medicinal herb *Paeonia suffruticosa* and its active constituent 1,2,3,4,6-penta-*O*-galloyl-β-D-glucopyranose have potent anti-aggregation effects on Alzheimer's amyloid β proteins *in vitro* and *in vivo*

Hironori Fujiwara,* Masahiro Tabuchi,† Takuji Yamaguchi,† Koh Iwasaki,* Katsutoshi Furukawa,‡ Kyoji Sekiguchi,† Yasushi Ikarashi,† Yukitsuka Kudo,§ Makoto Higuchi,¶,** Takaomi C. Saido,** Sumihiro Maeda,†† Akihiko Takashima,†† Masahiko Hara,‡‡ Nobuo Yaegashi,* Yoshio Kase† and Hiroyuki Arai‡

*Center for Asian Traditional Medicine, Tohoku University Graduate School of Medicine, Sendai, Aoba-ku, Japan

†TSUMURA Research Laboratories, TSUMURA & Co., Ibaraki, Japan

‡Department of Geriatrics and Gerontology, Division of Brain Sciences, Institute of Development, Aging and Cancer, Tohoku University, Aoba-ku, Sendai, Japan

§Innovation of Biomedical Engineering Center, Tohoku University, Aoba-ku, Sendai, Japan

¶Molecular Imaging Center, National Institute of Radiological Sciences, Inage-ku, Chiba, Japan

**Laboratory for Proteolytic Neuroscience, RIKEN Brain Science Institute, Wako, Saitama, Japan

††Laboratory for Alzheimer's Disease, RIKEN Brain Science Institute, Wako, Saitama, Japan

‡‡Local Spatio-Temporal Functions Laboratory, RIKEN Frontier Research System, Wako, Saitama, Japan

Abstract

The deposition of amyloid β (Aβ) protein is a consistent pathological hallmark of Alzheimer's disease (AD) brains; therefore, inhibition of Aβ fibril formation and destabilization of pre-formed Aβ fibrils is an attractive therapeutic and preventive strategy in the development of disease-modifying drugs for AD. This study demonstrated that *Paeonia suffruticosa*, a traditional medicinal herb, not only inhibited fibril formation of both $A\beta_{1-40}$ and $A\beta_{1-42}$ but it also destabilized pre-formed Aβ fibrils in a concentration-dependent manner. Memory function was examined using the passive-avoidance task followed by measurement of Aβ burden in the brains of Tg2576 transgenic mice. The herb improved long-term memory impairment in the transgenic mice and inhibited the accumulation of Aβ in the brain. Three-dimensional HPLC analysis revealed that a water extract of the herb contained several different chemical compounds including 1,2,3,4,6-penta-*O*-galloyl-β-D-glucopyranose (PGG). No obvious adverse/toxic were found following treatment with PGG. As was observed with *Paeonia suffruticosa*, PGG alone inhibited Aβ fibril formation and destabilized pre-formed Aβ fibrils *in vitro* and *in vivo*. Our results suggest that both *Paeonia suffruticosa* and its active constituent PGG have strong inhibitory effects on formation of Aβ fibrils *in vitro* and *in vivo*. PGG is likely to be a safe and promising lead compound in the development of disease-modifying drugs to prevent and/or cure AD.

Keywords: 1,2,3,4,6-penta-*O*-galloyl-β-D-glucopyranose, Alzheimer's disease, amyloid β protein, medicinal herb, *Paeonia suffruticosa*, Tg2576 transgenic mice.

J. Neurochem. (2009) **109**, 1648–1657.

Received November 27, 2008; revised manuscript received March 10, 2009; accepted March 23, 2009.

Address correspondence and reprint requests to Hiroyuki Arai, M.D., Ph.D., Department of Geriatrics and Gerontology, Division of Brain Sciences, Institute of Development, Aging and Cancer, Tohoku University, 4-1 Seiryo-cho Aobaku, Sendai 980-8575, Japan.
E-mail: harai@idac.tohoku.ac.jp

Abbreviations used: AD, Alzheimer's disease; APP, amyloid precursor protein; Aβ, amyloid β; MTT, 3-(4,5-dimethylthiazol-2-yl)-2,5-diphenyltetrazolium bromide; PGG, 1,2,3,4,6-penta-*O*-galloyl-β-D-glucopyranose.

Alzheimer's disease (AD) is the most prevalent cause of dementia and is characterized by loss of memory and cognition as well as behavioral and occupational instability in old age. One of the pathological characteristics of AD is the progressive deposition of insoluble amyloid β protein (Aβ) as a form of senile plaques (Wirths *et al.* 2004). This protein comprises peptides of approximately 39 to 43 amino acid residues derived from the transmembrane amyloid precursor protein (APP) (Selkoe 2002). Aβ can form monomers and a variety of different aggregate morphologies including dimers, small soluble oligomers, protofibrils, diffuse plaques, and fibrillar deposits seen in the senile plaques. Protofibrils, diffuse plaques, and fibrillar deposits seem to have a predominant β-sheet structure (Tierney *et al.* 1988; Barrow and Zagorski 1991), while oligomers are believed to be more globular (Barghorn *et al.* 2005). Increasing evidence that the formation of these aggregates, particularly oligomer, causes primary neurodegeneration in AD has led to the amyloid hypothesis which states that the accumulation of Aβ in the CNS is highly neurotoxic and deteriorates synaptic functions (Selkoe 2002; Wirths *et al.* 2004). Moreover, several lines of evidence suggest that Aβ accumulation begins at relatively early stages before cognitive decline becomes manifest (Anderton *et al.* 1998; Selkoe 2002). Therefore, it is hypothesized that the formation, deposition, and aggregation of Aβ in the brain should be primary targets for complete amelioration of dementia. Currently, drugs available for dementia such as acetylcholinesterase inhibitors exert only a temporary benefit on cognitive dysfunction (Millard and Broomfield 1995; Park *et al.* 2000; Darreh-Shori *et al.* 2004), and they do not prevent or reverse the formation of Aβ deposits. One potentially promising strategy for developing more effective anti-dementia drugs is the inhibition of Aβ fibril formation or destabilization of aggregated Aβ or a combination of both.

Herbal remedies are used worldwide and have a long history of use in alleviating a variety of symptoms of many different conditions and diseases. Recently, clinical trials in AD patients have also shown that some of these traditional medications improved Mini-Mental State Examination scores, P300 latency, and blood flow in the cerebral cortex (Le Bars *et al.* 1997). Although inconclusive, these provocative studies suggest that even old remedies can be beneficial in AD and related disorders. We have reported that several traditional herbal medicines such as *Formula lienalis angelicae compositae* (kamiuntanto) (Suzuki *et al.* 2001; Nakagawasai *et al.* 2004), *Pilulae octo-medicamentorum rehmanniae* (hachimijiogan) (Iwasaki *et al.* 2004), and *Pulvis depressionis hepatis* (yokukansan) (Iwasaki *et al.* 2005) improved symptoms of dementia. The radicis cortex of *Paeonia suffruticosa* (*Moutan cortex*; Botan-pi), a major medicinal plant comprising *Pilulae octo-medicamentorum rehmanniae*, is used as an anti-pyretic and anti-inflammatory agent (Lin *et al.* 1999; Yasuda *et al.* 1999; Chou 2003). Paeonol, a common component of *Paeonia suffruticosa*, has been shown to inhibit platelet aggregation in rabbits (Lin *et al.* 1999) as well as to reduce cerebral infarction in ischemia-reperfusion-injured rats (Hsieh *et al.* 2006). However, the underlying mechanism of traditional medicinal herbs, including *Paeonia suffruticosa*, on the formation and metabolism of Aβ fibrils has never been investigated. In the present study, we examined the effect of *Paeonia suffruticosa* on the formation of Aβ aggregates and its ability to destabilize pre-formed Aβ fibrils *in vitro* by using fluorescence spectroscopy with thioflavin T.

1,2,3,4,6-Penta-*O*-galloyl-β-D-glucopyranose (PGG), a high molecular weight tannin-type polyphenols, has been isolated from *Paeonia suffruticosa*. The defining characteristic of tannins is their ability to bind and precipitate proteins (Hofmann *et al.* 2006). Li *et al.* (2005) previously reported that PGG could bind to insulin receptors and activate an insulin-mediated glucose transport signaling pathway. However, the effect of this compound on the formation and metabolism of Aβ fibrils has not yet been investigated.

Our results provide strong evidence that several traditional herbs extracts including *Paeonia suffruticosa* and PGG have inhibitory and destabilizing effects on Aβ fibrils.

Materials and methods

Reagents

Aβ peptides (1–40 and 1–42) and thioflavin-T were obtained from Peptide Institute (Osaka, Japan) and from Sigma (St Louis, MO, USA), respectively. All the reagents and drugs used were of analytical grade.

Preparation of medicinal herb extracts

Water, 100% methanol, and 99.5% ethanol extracts of medicinal herbs were prepared by refluxing 10 g of sliced dry herbs in 100 mL of each solution for 30 min. The decoction after cooling to 25°C was evaporated completely under reduced pressure to yield dried or oily extracts. The extracts were weighed and dissolved in dimethylsulfoxide at a concentration of 100 mg/mL and then stored at −20°C. When assaying, these extracts were dissolved in 50 mM potassium phosphate buffer (pH 7.4) and the solutions were adjusted to pH 7.4 when necessary.

Analysis of three-dimensional HPLC fingerprints of water extract of *Paeonia suffruticosa*

Paeonia suffruticosa (0.5 g) was extracted with 30 mL of distilled water under ultrasonication for 30 min. The solution was filtered and then analyzed by HPLC. The HPLC system consisted of an HPLC pump (LC-10AD; Shimadzu, Kyoto, Japan) and a TSK-GEL 80_{TS} column (4.6 mm × 250 mm), and (A) 50 mM acetic acid-ammonium acetate and (B) acetonitrile were used as the eluents. A linear gradient of 90% A and 10% B changing over 60 min to 0% A and 100% B was used. The flow rate was controlled at 1.0 mL/min. After the eluate was obtained from the column, the three-dimensional data were processed with a diode array detector (SPD-M10A; Shimadzu).

Thioflavin-T measurement

Thioflavin-T measurement was performed using the method described by Suemoto *et al.* (2004) with slight modifications. For the Aβ aggregate-formation assay, Aβ (20 μM) dissolved in the 50 mM potassium phosphate buffer (pH 7.4) with a test herbal extract was incubated at 37°C for 96 h ($A\beta_{1-40}$) or 24 h ($A\beta_{1-42}$). For the destabilization assay of pre-formed Aβ aggregates, after incubation of $A\beta_{1-40}$ (96 h) or $A\beta_{1-42}$ (24 h) without a test herbal extract, a mixture of the aggregated Aβ and a test herbal extract was incubated for 30 min at 37°C.

At the end of the incubation, 3 μM thioflavin-T dissolved in 100 mM glycine buffer (pH 8.5) was added to the mixture. Fluorescence of thioflavin-T bound to Aβ aggregates was measured using a microplate reader (Spectramax GEMINI XS; Molecular Devices, Sunnyvale, CA, USA) (excitation at 442 nm and emission at 485 nm) after incubation for 30 min at 25°C. The percentage inhibition was calculated by comparing the fluorescence values of test samples with those of control solutions without herbal extracts.

Animals

Tg2576 APPswe mice over-express a 695-amino acid splice form (Swedish mutation K670N M671I) of the human Aβ precursor protein (APP695) which resulted in a fivefold increase in $A\beta_{1-40}$ and a 14-fold increase in $A\beta_{1-42}$ with increasing age, driven by the hamster prion protein promoter. The animals were allowed free access to water and standard laboratory food in a facility with the temperature controlled at 24 ± 1°C and relative humidity at 55 ± 5%, with lights on from 7:00 to 19:00 hours daily. Behavioral studies were performed between 10:00 and 12:00 hours. Experimental protocols were approved by the Animal Care and Use Committee, Tohoku University Graduate School of Medicine, and complied with the procedures outlined in the Guide for the Care and Use of Laboratory Animals of Tohoku University.

Step-through passive-avoidance test

The apparatus (AP model; O'Hara Co., Tokyo, Japan) for the step-through passive-avoidance test consisted of two compartments, illuminated compartment [100 mm × 120 mm × 100 mm; light at the top of compartment (27W, 3000 lx)] and dark compartment (100 mm × 170 mm × 100 mm). The compartments were separated by a guillotine door. During the learning stage, a mouse was placed in the illuminated safe compartment. As the compartment was lit, the mouse stepped through the opened guillotine door into the dark compartment. The time spent in the illuminated compartment was defined as the latency time. Three seconds after the mouse entered the dark compartment, a foot shock (0.3 mA, 50V, 50 Hz ac, for 3 s) was delivered to the floor grids in the dark compartment. The mouse could escape from the shock only by stepping back to the safe illuminated compartment. Such acquisition trials during the learning stage were carried out once a day for 5 days. It was judged as learning avoidance from foot-shock if the mouse remained in the illuminated compartment for 300 s after being placed there. The retention trials were carried out once per week for 10 weeks from Days 8 to 78 to evaluate the retention of avoidance memory. The latency time was measured for up to 300 s without delivering foot-shock. It was judged that the mouse retained the avoidance memory when it stayed in the illuminated safe compartment for 300 s. Acquisition and retention trials were conducted in 11-month-old mice.

Immunocytochemistry

All sample brains were fixed in neutral-buffered formalin and embedded in paraffin. Immunocytochemistry was performed using an Amyloid β Protein Immunohistostain Kit (Wako Pure Chemical Industries, Ltd., Osaka, Japan) according to the manufacturer's instructions. Briefly, after deparaffinization, 8-μm brain sections were immersed in 99% formic acid for 5 min, blocked with blocking serum, and immunostained with BA27 ($A\beta_{1-40}$) and BC05 ($A\beta_{1-42}$) by a standard avidin–biotin complex method, using 3,3′-diaminobenzidine as chromogen and lightly counter-staining with hematoxylin.

Tissue preparation

Tissue samples were processed in Tris-buffered saline (soluble fraction) and 70% formic acid (insoluble fraction) containing 1× protease inhibitor mixtures as described previously (Calon *et al.* 2004) with slight modifications. Briefly, brain tissues were homogenized and sonicated in Tris-buffered saline containing protease inhibitor mixture. The resulting homogenate was subjected to ultracentrifugation at 200 000 *g* at 4°C for 20 min, and the soluble supernatant was collected and frozen. To analyze the insoluble Aβ, the insoluble pellet was sonicated in 200 μL of 70% formic acid and subjected to ultracentrifugation at 300 000 *g* at 4°C for 30 min, and the soluble supernatant was collected.

Aβ levels

Brain $A\beta_{1-40}$ and $A\beta_{1-42}$ levels were measured using sandwich ELISA with a Human β Amyloid ELISA Kit (Wako Pure Chemical Industries, Ltd.) according to the manufacturer's instructions. BAN50 is a monoclonal antibody raised against a synthetic peptide of human $A\beta_{1-16}$; it preferentially reacts with the N-terminal portion of human Aβ starting at Asp-1 but does not cross-react with N-terminally truncated Aβ nor with rodent-type Aβ. BA27 and BC05, which specifically recognize the C terminus of $A\beta_{1-40}$ and $A\beta_{1-42}$, respectively, were conjugated with horseradish peroxidase and used as detector antibodies. Mice brain insoluble fractions described above were neutralized and subjected to BAN50/BA27 or BAN50/BC05 ELISA. The amount of Aβ was calculated by comparing these absorbance values with those of control solutions without herbal extract.

Aβ ologomerization analysis

Amount of $A\beta_{1-42}$ oligomer was measured using Aβ Aggregate Human Singleplex Bead Kit (Invitrogen Corporation, Carlsbad, CA, USA) according to the manufacturer's instructions. Data analysis was performed by a flow cytometer (FACSCaliber, Becton Dickinson Immunocytometry Systems, Franklin Lakes, NJ, USA).

Cell viability assay

SK-N-SH cells were maintained in Dulbecco's modified Eagle's medium (Gibco Life Technologies, Carlsbad, CA, USA) supplemented with 10% fetal calf serum and 4 mM L-glutamine in a humidified atmosphere of 5% CO_2 and 95% air. SK-N-SH cells were seeded in 96-well plates at a density of 1×10^4 cells per well. After 24 h, we pre-incubated SK-N-SH cells for 30 min with PGG, followed by 24 h treatment with 10 μM aggregated $A\beta_{1-42}$. Cell

viability was assessed using the 3-(4,5-dimethylthiazol-2-yl)-2,5-diphenyltetrazolium bromide (MTT) method. Absorbance values of formazan were determined at 590 nm with an automatic microplate reader.

Data analysis

Data were expressed as mean ± SD. Statistical comparisons were made using ANOVA with Bonferroni's *post hoc* analysis. $p < 0.05$ was considered to be significant.

Results

Concentration-dependent effects of *Paeonia suffruticosa* on kinetics of Aβ fibril formation and breakdown

In our previous publication, it was noted that several medicinal herbs including *Uncaria rhynchophylla*, *Cinnamomum cassia*, and *Paeonia suffruticosa* showed destabilizing activity on Aβ fibrils (Fujiwara *et al.* 2006). *Paeonia suffruticosa* which was extracted either by water, methanol, or ethanol was concentrated under reduced pressure to yield oily residues (2.33, 1.89, and 2.14 g for water, methanol, and ethanol, respectively). To examine the inhibitory effect of *Paeonia suffruticosa* on Aβ fibril formation, concentration-dependencies were examined by the thioflavin T method. We observed that fluorescence intensity in $A\beta_{1\text{-}40}$ and $A\beta_{1\text{-}42}$ declined in a concentration-dependent manner (Fig. 1a and b). $A\beta_{1\text{-}40}$ fibril formation was inhibited by 10 μg/mL of the water (48.5 ± 0.3%), methanol (40.1 ± 2.8%), and ethanol (34.6 ± 0.2%) extracts of *Paeonia suffruticosa*. $A\beta_{1\text{-}42}$ fibril formation was also inhibited by each of the three different extracts (10 μg/mL), although the inhibitory concentration was lower than for $A\beta_{1\text{-}40}$.

In the analysis of fibril destabilization, fluorescence derived from thioflavin T was decreased in a dose-dependent manner after the addition of each of the extracts of *Paeonia suffruticosa* to pre-formed Aβ fibrils, and the degree of inhibition was similar to that observed on Aβ aggregation (Fig. 1c and d). Pre-formed $A\beta_{1\text{-}40}$ fibrils were destabilized by 10 μg/mL of the water (58.2 ± 3.7%), methanol (74.9 ± 1.1%) and ethanol (71.7 ± 1.0%) extracts. Over 80% of pre-formed $A\beta_{1\text{-}40}$ and $A\beta_{1\text{-}42}$ fibrils were destabilized by each of the three different extracts at the concentration of 100 μg/mL.

Step-through passive-avoidance tests

Step-through passive-avoidance tests were carried out in Tg2576 mice at 11 to 14 months of age. In the first acquisition trial of the learning stage, all mice (11 months

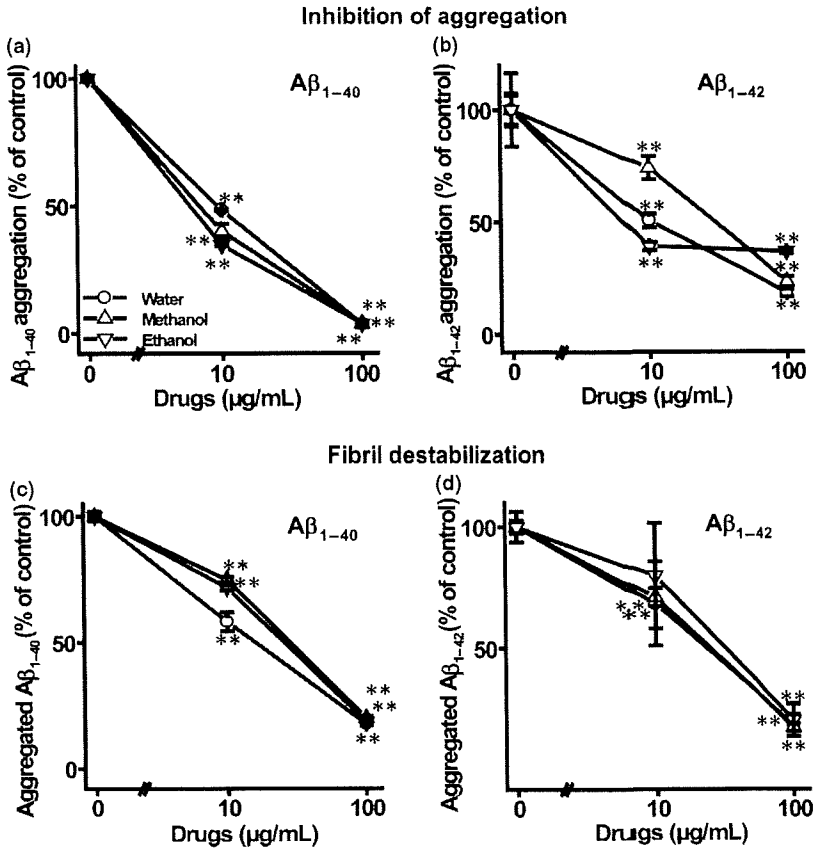

Fig. 1 Effects of three different *Paeonia suffruticosa* extracts on the kinetics of Aβ formation and destabilization. a and b: Aβ aggregate-formation assay. Reaction mixtures containing 20 μM of $A\beta_{1\text{-}40}$ (a) or $A\beta_{1\text{-}42}$, (b) 50 mM phosphate buffer (pH 7.4), and various extracts [water (circles), methanol (upward-pointing triangles), and ethanol (downward-pointing triangles)] were incubated at 37°C for 96 h (a) or 24 h (b). Aβ aggregation was expressed as percentage of the control sample which did not contain herbal extract. c and d: Aβ aggregate-destabilization assay. Reaction mixtures containing 20 μM $A\beta_{1\text{-}40}$ (c) or $A\beta_{1\text{-}42}$ (d) were incubated at 37°C for 96 h (c) or 24 h (d). The extracts were then added and incubated for another 30 min. Aβ aggregation was assessed by the thioflavin T method and expressed as the percentage of control aggregation in the absence of herbal extract. Values represent mean ± SD from four independent experiments. $^{**}p < 0.01$ compared with extract-untreated control.

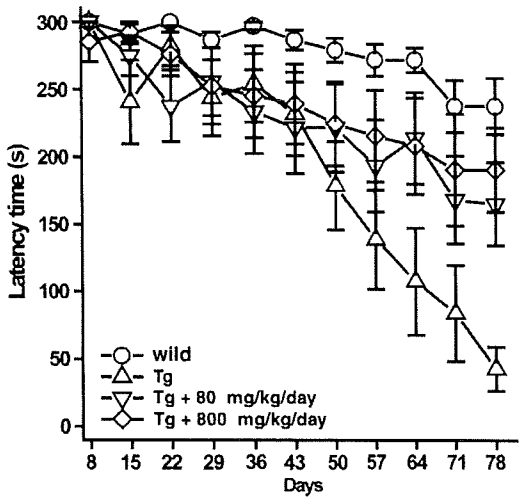

Fig. 2 Step-through latencies in the retention stages of the passive-avoidance task in *Paeonia suffruticosa*-treated transgenic (Tg2576) mice. Wild type and transgenic mice could acquire the avoidance memory by four or five repeated learning trials. The retention trials were carried out once per week for 10 weeks from Days 8 to 78 to evaluate the retention of avoidance memory. The latency time was measured for up to 300 s without delivering foot-shock. Wild type (Wild: circles); transgenic mice (Tg: upward-pointing triangles); 80 mg/kg/day *Paeonia suffruticosa* by repeated oral administration (Tg + 80 mg/kg/day: downward-pointing triangles), and 800 mg/kg/day *Paeonia suffruticosa* (Tg + 800 mg/kg/day: diamond). Values represent the means ± SD from 11 to 17 independent experiments.

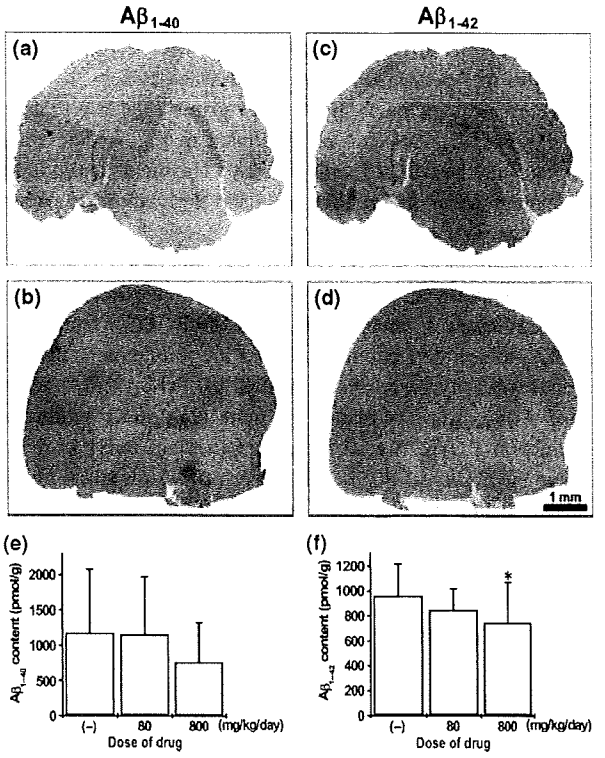

Fig. 3 Immunostaining (a–d) and ELISA analysis of formic acid-extractable Aβ levels (e and f) after dietary intake of *Paeonia suffruticosa* in Tg2576 mice. (a–d) Hemibrain cryostat sections were labeled with anti-$A\beta_{1-40}$ (a and b) and $A\beta_{1-42}$ (c and d) antibody. Image analysis was performed on the cerebral cortex from untreated (a and c) and *Paeonia suffruticosa*-treated (b and d) animals. Scale bar = 1 mm. Levels of $A\beta_{1-40}$ (e) and $A\beta_{1-42}$ (f) were quantified using an ELISA kit on formic acid-extractable Aβ from cortices of the low intake group (80 mg/kg/day) and high intake group (800 mg/kg/day). Values represent mean ± SD from 11 to 17 independent experiments. *$p < 0.05$ compared with *Paeonia suffruticosa*-untreated control.

old) in the wild type and Tg groups entered the dark compartment immediately after being placed in the illuminated compartment. Repeating the acquisition trial increased the latency times in both groups. All mice in the wild type and Tg groups acquired avoidance memory, staying in the illuminated compartment for over 300 s on the fifth acquisition day. However, no significant differences were observed in the mean latency times between the wild type and Tg groups on any given day during the learning stage (data not shown). In retention trials (Fig. 2), the step-through latency of the Tg group was significantly reduced when compared with that of the wild type group. *Paeonia suffruticosa*-treated Tg mice were indistinguishable from non-transgenic littermates on days from 50 to 78 of testing.

Aβ pathology was reduced in *Paeonia suffruticosa*-treated Tg mice

To determine whether oral *Paeonia suffruticosa* treatment affected the accumulation of Aβ in brain tissue, we evaluated Aβ immunoreactivity in brain sections from untreated (Fig. 3a and c) and *Paeonia suffruticosa*-treated mice (Fig. 3b and d) using BA27 and BC05 antibodies which recognize the C-terminus of human $A\beta_{1\ 40}$ (Fig. 3a and b) and $A\beta_{1\ 42}$ (Fig. 3c and d). The number of Aβ-positive spots in the cortex and hippocampus were obviously lower in the *Paeonia suffruticosa*-treated mice compared with the untreated mice. No Aβ immunoreactivity was observed in brain sections from non-transgenic mice (data not shown).

We next measured the levels of $A\beta_{1\ 40}$ and $A\beta_{1\ 42}$ in brain tissue samples from Tg mice using a sensitive ELISA method (Fig. 3e and f). Consistent with the results of Aβ immunostaining, the $A\beta_{1\ 42}$ concentration in the samples from *Paeonia suffruticosa*-treated Tg mice (800 mg/kg/day) was significantly lower than the concentration in *Paeonia suffruticosa*-untreated mice (747.8 ± 322.4%, $p < 0.05$). In contrast to its effect on $A\beta_{1\ 42}$ levels, *Paeonia suffruticosa* treatment had no significant effect on $A\beta_{1\ 40}$ levels in the Tg mice. The levels of $A\beta_{1\ 40}$ and $A\beta_{1\ 42}$ were below the limit of detection in cerebral cortex samples from non-transgenic mice (data not shown).

HPLC analyses of *Paeonia suffruticosa*: identification of four different natural compounds and their effects on the kinetics of $A\beta_{1-42}$ formation and destabilization

The three-dimensional-HPLC fingerprints of water extracts of *Paeonia suffruticosa* are illustrated in Fig. 4. The water extract contained several different chemical compounds including paeonol, benzoic acid, and derivatives of paeoniflorin as well as PGG.

Concentration dependence of the inhibitory effects of these compounds on Aβ fibril formation was examined using the thioflavin T method (Fig. 5a). Only PGG induced a concentration-dependent decline in the thioflavin T fluorescence intensity associated with $A\beta_{1-42}$. PGG (3 μM) inhibited $A\beta_{1-42}$ fibril formation by more than 50%. Additional thioflavin-T experiments were performed in order to determine the ability of PGG to destabilize pre-formed Aβ fibrils. Fluorescence derived from thioflavin T was decreased in a dose-dependent manner after the addition of PGG to pre-formed Aβ fibrils to an extent similar to that seen for the inhibition of Aβ aggregation (Fig. 5b).

Next, we incubated different concentrations of PGG with unpolymerized $A\beta_{1-42}$ (10 μM) and monitored the formation of amyloid using the Thioflavin T method (Fig. 6). In the absence of PGG, $A\beta_{1-42}$ formed Thioflavin T-binding aggregates after a lag phase of 2 h, whereas thioflavin T signals were decreased to 33.6 ± 16.8% by 1 μM PGG after a lag phase of 24 h. Moreover, $A\beta_{1-42}$ aggregation was completely inhibited by 100 μM PGG.

Effect of PGG on $A\beta_{1-42}$ oligomers

To further characterize the breakdown products that accumulated in the presence of PGG, aliquots of $A\beta_{1-42}$ oligomerization reaction mixtures in the presence or absence of PGG were assayed by flow cytometric analysis (Fig. 7). In the absence of PGG, the fluorescence intensity of $A\beta_{1-42}$ oligomerized sample was potent compared with vehicle sample without $A\beta_{1-42}$ oligomers (Fig. 7a and b). Samples treated with PGG reduced the fluorescence intensity in a concentration-dependent manner (Fig. 7c–e). These data confirmed that PGG was a strong inhibitor of $A\beta_{1-42}$ oligomerization.

Neuroprotective effects of PGG against Aβ toxicity

To evaluate whether PGG could potentially prevent Aβ-induced toxicity, we pre-incubated SK-N-SH cells for 30 min with PGG, followed by 24 h treatment with 10 μM aggregated $A\beta_{1-42}$. SK-N-SH cell viability was significantly impaired by Aβ peptides, measured by MTT assay. PGG (10 μM) significantly protected SK-N-SH cells against Aβ-induced toxicity. When measured by MTT reduction, cell survival was restored from 56.9 ± 2.5% to 87.0 ± 13.6% in response to the $A\beta_{1-42}$ aggregates (Fig. 8).

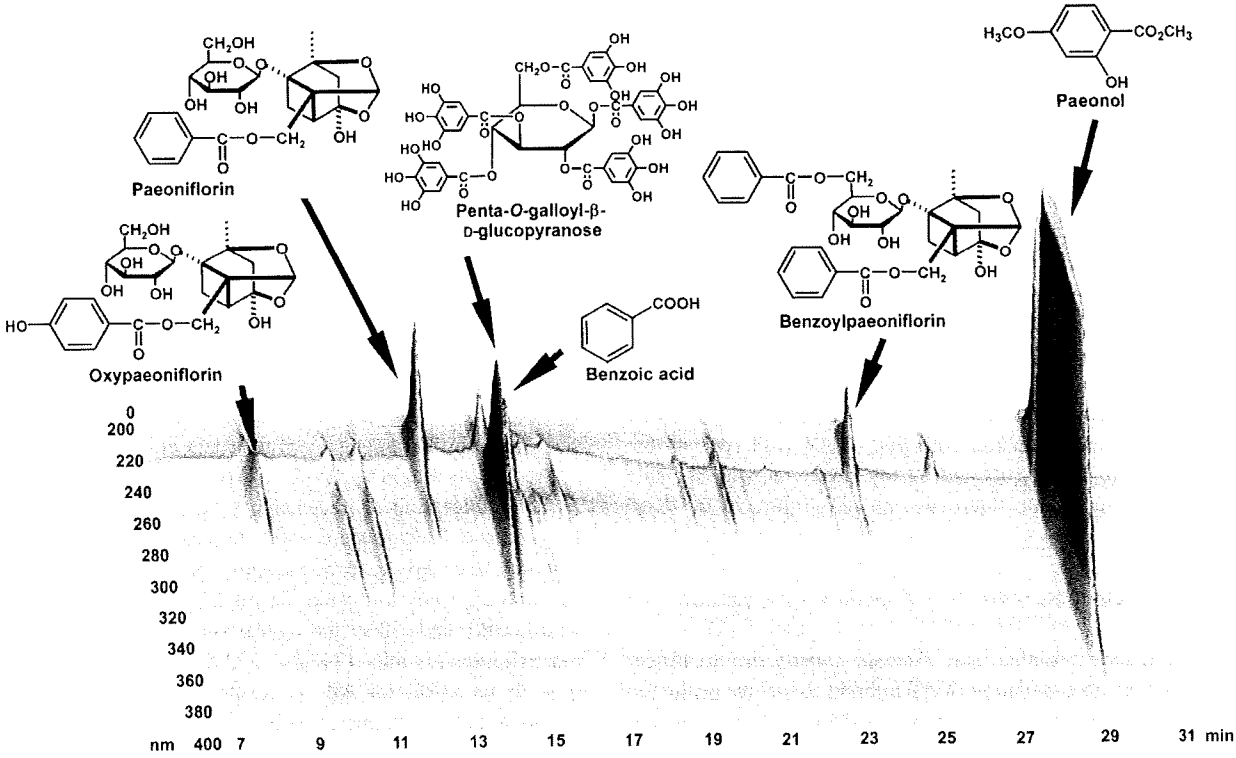

Fig. 4 Identification of chemicals by three-dimensional HPLC analysis of the water extract of *Paeonia suffruticosa*. Each peak indicates a molecule described in the figure.

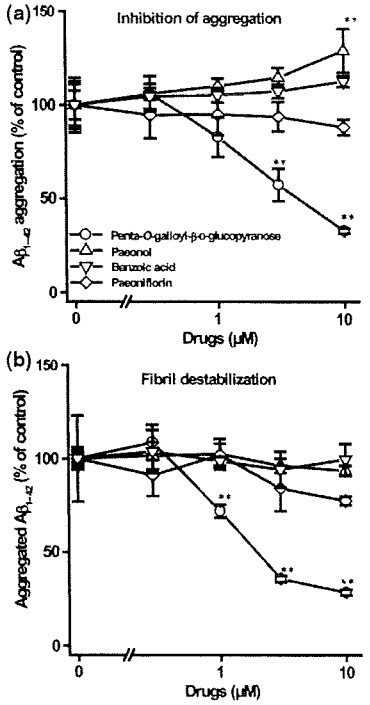

Fig. 5 Effects of distinct compounds isolated from *Paeonia suffruticosa* on the kinetics of Aβs formation and destabilization. a: Aβ aggregate-formation assay. Reaction mixtures containing 20 μM of $A\beta_{1-42}$, 50 mM phosphate buffer (pH 7.4), and various compounds [1,2,3,4,6-penta-*O*-galloyl-β-D-glucopyranose (circles), paeonol (upward-pointing triangles), benzoic acid (downward-pointing triangles), and paeoniflorin (diamond)] were incubated at 37°C for 24 h. Aβ aggregation is expressed as percentage of control observed in the absence of test compounds. b: Aβ aggregate-destabilization assay. Reaction mixtures containing 20 μM $A\beta_{1-42}$ were incubated at 37°C for 24 h. The extracts were added and incubated for 30 min. Aβ aggregation was assessed by the thioflavin T method and expressed as percentage of control aggregation observed in the absence of test compounds. Values represent mean ± SD from four independent experiments. $^{**}p < 0.01$ compared with extract-untreated control.

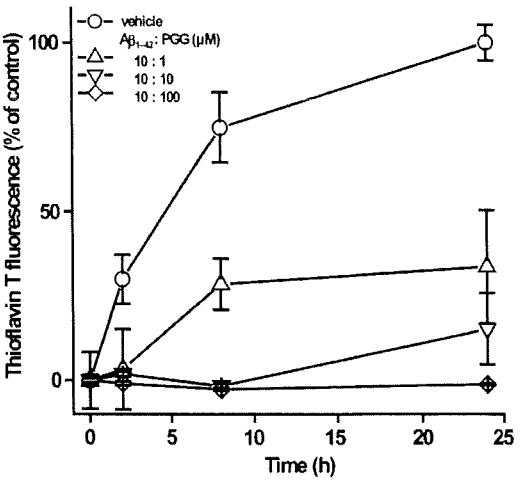

Fig. 6 The molar ratio of the Aβ–PGG interaction. Reaction mixtures containing 10 μM $A\beta_{1-42}$: PGG [solvent alone (circles), molar ratio 10 : 1 (upward-pointing triangles), 10 : 10 (downward-pointing triangles), and 10 : 100 (diamond)] were incubated at 37°C for indicated time. Thioflavin T fluorescence was expressed as a percentage of control which was observed at the point of 24 h without PGG. Values represent mean ± SD from four independent experiments.

Aβ pathology is diminished in PGG-treated Tg mice

To determine the effect of oral PGG treatment accumulation of Aβ in Tg type mice, we evaluated Aβ immunoreactivity in brain sections from untreated and PGG-treated mice by using antibodies BA27 and BC05 (Fig. 9a–d). The number of Aβ-positive spots in the hippocampus was obviously lower in PGG-treated mice (Fig. 9b and d) compared with untreated mice (Fig. 9a and c). No Aβ immunoreactivity was observed in brain sections from non-transgenic mice (data not shown).

We next measured the levels of $A\beta_{1\ 40}$ and $A\beta_{1\ 42}$ in brain samples from Tg mice by using a sensitive ELISA method (Fig. 9e and f). In the brains of Tg mice treated with PGG by repeated oral administration, the $A\beta_{1\ 40}$ and $A\beta_{1\ 42}$ concentrations were significantly lower (2417.5 ± 279.5% and 46.8 ± 3.0%, $p < 0.01$) than those in PGG-untreated mice. The levels of $A\beta_{1\ 40}$ and $A\beta_{1\ 42}$ were below the limit of detection in cerebral cortex samples from non-transgenic mice (data not shown).

Discussion

In AD research, much attention has focused on altering the course of the disease through early diagnosis and intervention. Clinical application of biomarkers and amyloid imaging may be attractive and realistic diagnostic procedures by which to identify the disease early. On the other hand, safety is an important concern with regard to early intervention with disease modifying drugs. *Paeonia suffruticosa* has been used medicinally in humans for more than 1000 years with virtually no toxic effects reported.

The results of our studies using thioflavin T fluorescence demonstrated that *Paeonia suffruticosa* extracts, regardless of the extraction method used, could inhibit the assembly of Aβ fibrils. All three extracts (water, methanol, and ethanol) induced a dramatic decline in the fluorescence intensity of thioflavin T in the μg/mL range. In our preliminary experiment, we confirmed that these extracts did not quench thioflavin T fluorescence at the indicated concentrations. These results suggest two possibilities; one is that *Paeonia suffruticosa* indeed destabilizes Aβ fibrils, and the other is that it antagonizes the binding of thioflavin T to Aβ. It has been reported that absorbance of Congo red was increased by binding to Aβ protein as well as to thioflavin T. The binding site in Aβ to Congo red was different from that to thioflavin

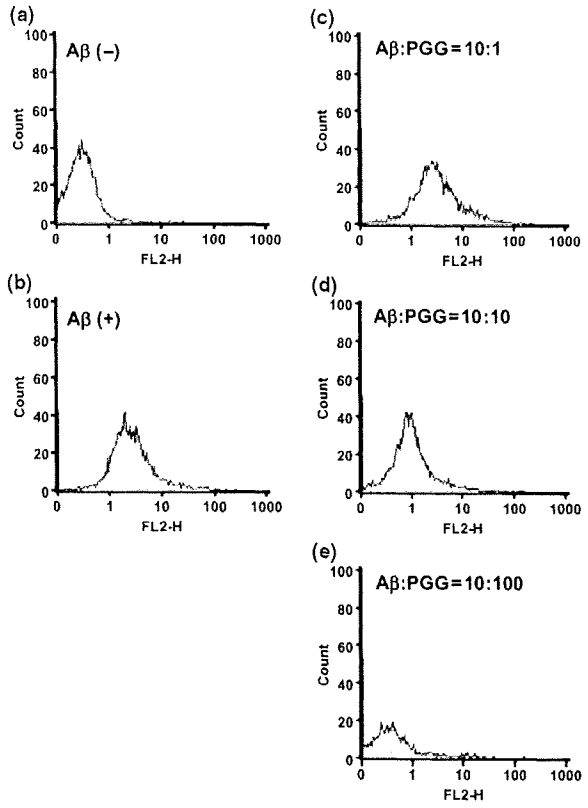

Fig. 7 Effects of PGG on $A\beta_{1-42}$ oligomeric species. These histograms were developed using reagents provided in the Aggregated Aβ Assay Kit. a: buffer-control; b: 10 μM $A\beta_{1-42}$ in absent of PGG; c–e: 10 μM $A\beta_{1-42}$ with PGG molar ratio 10 : 1 (c), 10 : 10 (d), and 10 : 100 (e).

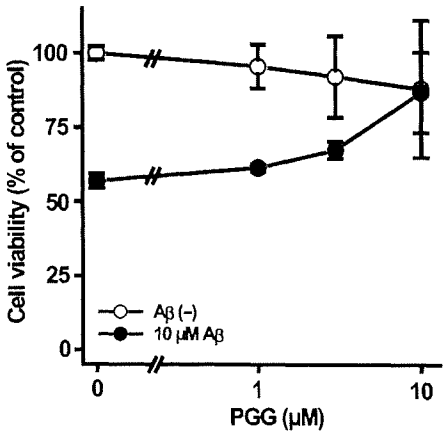

Fig. 8 Effects of PGG against Aβ-induced toxicity. SK-N-SH cells were pre-treated without or with PGG for 30 min followed by incubation without or with $A\beta_{1-42}$ (10 μM) for 24 h. Cell viability was assessed by MTT method and expressed as a percentage of control viability, which was observed in the absence of $A\beta_{1-42}$ and PGG. Values represent the means ± SD from four independent experiments.

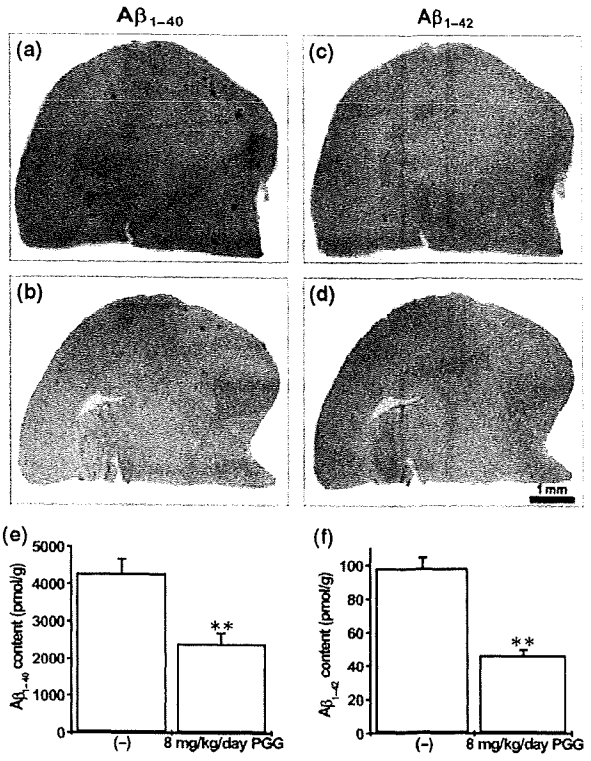

Fig. 9 Immunostaining (a–d) and ELISA analysis of formic acid-extractable Aβ levels (e and f) after dietary intake of 1,2,3,4,6-penta-*O*-galloyl-β-D-glucopyranose (PGG) in Tg2576 mice. (a–d) Hemibrain cryostat sections were labeled with anti- $A\beta_{1-40}$ (a and b) and $A\beta_{1-42}$ (c and d) antibody. Image analysis was performed on the cerebral cortices from PGG-untreated (a and c) and -treated (b and d) animals. Scale bar = 1 mm. Levels of $A\beta_{1-40}$ (e) and $A\beta_{1-42}$ (f) were quantified on formic acid-extractable Aβ from cortices of the 8 mg/kg/day PGG groups. Values represent mean ± SD from seven to eight independent experiments. $^{**}p < 0.01$, compared with PGG-untreated control.

T. In our experiments, each of the three *Paeonia suffruticosa* extracts decreased the absorbance of Congo red (data not shown), suggesting that the decrease in thioflavin T fluorescence by *Paeonia suffruticosa* extracts was caused by destabilization of Aβ fibrils. Moreover, our preliminary atomic force microscopy data also strongly support this notion, as destabilization of Aβ fibrils by *Paeonia suffruticosa* extracts was directly visualized (data not shown). The extracts of *Paeonia suffruticosa* inhibited aggregation of both $A\beta_{1-40}$ and $A\beta_{1-42}$ to a similar extent. Therefore, the inhibitory effect of *Paeonia suffruticosa* on amyloidogenesis of Aβ may not be dependent on the distinct amino acid sequence of its C-terminal.

Paeonia suffruticosa treatment prevented Aβ-related memory deficits and AD-type neuropathology *in vivo*. In our study, we found that treatment of Tg2576 mice with *Paeonia suffruticosa* attenuated memory deterioration, and this effect coincided with an approximately 20% reduction in

Aβ peptide content in the brain. We hypothesize that treatment with *Paeonia suffruticosa* may have beneficial effects on AD-type memory deterioration through a direct interaction between *Paeonia suffruticosa* and Aβ peptides in the brain, leading to the prevention of Aβ plaque formation.

Our studies also showed that PGG at low concentrations (IC_{50} = 3 μM) can inhibit Aβ aggregation or promote its destabilization. Moreover, our preliminary scanning electron microscopy data also strongly support this notion, as destabilization of Aβ fibrils by PGG was directly visualized (Fig. S1). As other chemical compounds, such as paeonol, benzoic acid, and paeoniflorin had no effects on Aβ aggregation, PGG may be the principal active constituent responsible for the effect of *Paeonia suffruticosa* on Aβ fibril regulation. Previous published literatures reported that several polyphenols, such as those from green tea or grape, had anti-aggregation property (Ehrnhoefer *et al.* 2008; Rivière *et al.* 2008). PGG had a comparable inhibitory effect with such published polyphenols.

The toxicity of Aβ is becoming more strongly linked to the formation of oligomeric aggregates (Kirkitadze *et al.* 2002). In our experiments, PGG inhibited Aβ oligomerization. Moreover, treatment of SK-N-SH cells with PGG significantly protected the cells from $Aβ_{1-42}$ toxicity at concentrations similar to those that inhibited Aβ aggregation. Thus, our experiments suggest that PGG inhibited not only Aβ fibril formation but also neurotoxic Aβ oligomer formation. Furthermore, oral intake of PGG reduced Aβ plaque burden and Aβ peptide content in brain tissue from Tg2576 mice, as did like *Paeonia suffruticosa*. There are two possible explanations; one is that PGG indeed destabilizes Aβ fibrils, and the other is that it inhibits the Aβ production or its secretion in Tg2576 mice brain. We demonstrated that PGG did not affect the level of full-length APP in Tg2576 mice (Figure S2), suggesting that the decrease in Aβ plaques and Aβ peptide content in brain tissue from Tg2576 mice by PGG may be caused by destabilization of Aβ fibrils. Curcumin, an active compound of *Curcuma longa*, was reported to inhibit Aβ fibril formation and to destabilize preformed Aβ fibrils *in vitro* and *in vivo* (Ono *et al.* 2004; Yang *et al.* 2005). It has also been reported that this compound is highly hydrophobic and should readily enter the brain to bind to plaques *in vivo* (Yang *et al.* 2005). Although highly hydrophilic, unlike curcumin, PGG has curcumin-like activity on Aβ fibril regulation *in vivo*. Studies of the metabolism of PGG and its ability to penetrate the blood-brain barrier by this compound are now underway.

In conclusion, our study demonstrates that *Paeonia suffruticosa* and PGG not only inhibit Aβ fibril formation but also disassemble pre-formed Aβ fibrils. Moreover, our experiments suggest that PGG inhibits Aβ oligomerization and Aβ toxicity. As a result, it improved memory deficits in Tg2576 mice. Therefore, extracts of *Paeonia suffruticosa* and PGG could have potential as therapeutic drugs for AD patients and may also be useful as primary or secondary preventive agents for healthy individuals and patients with mild cognitive impairment. Furthermore, *Paeonia suffruticosa* has a satisfactory safety profile because no obvious adverse effects of *Pilulae octo-medicamentorum rehmanniae* have been reported. In our preliminary experiments, *Paeonia suffruticosa* was tested for hepatotoxicity, nephrotoxicity, and other biochemical parameters in transgenic mice. Fortunately, this medicinal herb did not show any signs of organ toxicity. Thus, *Paeonia suffruticosa* appears to be a safe natural product for regulating Aβ aggregation. *Paeonia suffruticosa* and PGG may represent a new class of therapeutic and preventive agents for AD which act to regulate the formation and the clearance of senile plaques.

Acknowledgements

This work was partially supported by (i) a grant-in-aid for scientific research from the Ministry of Education, Science, Sports and Culture of Japan (#16590554), (ii) a program for the promotion of fundamental studies in Health Science of the National Institute of Biomedical Innovation (NIBIO) of Japan (#03-1), and (iii) a grant-in-aid from Core Research for Evolutional Science and Technology of Japan Science and Technology Corporation. We thank S. Isogami and M. Takahashi for kind advice and technical supports.

Supporting Information

Additional Supporting Information may be found in the online version of this article:

Figure S1 Scanning electron microscope imaging of $Aβ_{1-42}$ fibrils. After incubation of $Aβ_{1-42}$ for 24 h for preformed fibrils, the mixture of aggregated Aβ and the PGG was incubated at 37°C for 1 h. A: vehicle (DMSO); B: 10 μM $Aβ_{1-42}$: 10 μM PGG (molar ratio 1 : 1). Scale bar = 5 μm.

Figure S2 Effects of PGG on the level of amyloid precursor protein (APP) in Tg2576 mice. Immunoblotting of brain levels of APP after dietary 1,2,3,4,6-penta-*O*-galloyl-β-D-glucopyranose (PGG) in Tg2576. Levels of APP were quantitated by immunoblotting with full length APP antibody from cortices of 8 mg/kg/day-PGG groups. The samples were separated on a 10% polyacrylamide gel, followed by immunoblotting with anti-full length APP antibody. Arrowheads point to APP. Similar results were obtained from at least 3 independent experiments.

Please note: Wiley-Blackwell are not responsible for the content or functionality of any supporting materials supplied by the authors. Any queries (other than missing material) should be directed to the corresponding author for the article.

References

Anderton B. H., Callahan L., Coleman P. *et al.* (1998) Dendritic changes in Alzheimer's disease and factors that may underlie these changes. *Prog. Neurobiol.* **55**, 595–609.

Barghorn S., Nimmrich V., Striebinger A. *et al.* (2005) Globular amyloid beta-peptide oligomer – a homogenous and stable neuropathological protein in Alzheimer's disease. *J. Neurochem.* **95**, 834–847.

Barrow C. J. and Zagorski M. G. (1991) Solution Structures of β-peptide and its constituent fragments: relation to amyloid deposition. *Science* **253**, 179–182.

Calon F., Lim G. P., Yang F. *et al.* (2004) Docosahexaenoic acid protects from dendritic pathology in an Alzheimer's disease mouse model. *Neuron* **43**, 633–645.

Chou T. C. (2003) Anti-inflammatory and analgesic effects of Paeonol in carrageenan-evoked thermal hyperalgesia. *Br. J. Pharmacol.* **139**, 1146–1152.

Darreh-Shori T., Hellstrom-Lindahl E., Flores-Flores C. *et al.* (2004) Long-lasting acetylcholinesterase splice variations in anticholinesterase-treated Alzheimer's disease patients. *J. Neurochem.* **88**, 1102–1113.

Ehrnhoefer D. E., Bieschke J., Boeddrich A. *et al.* (2008) EGCG redirects amyloidogenic polypeptides into unstructured, off-pathway oligomers. *Nat. Struct. Mol. Biol.* **15**, 558–566.

Fujiwara H., Iwasaki K., Furukawa K. *et al.* (2006) *Uncaria rhynchophylla*, a Chinese medicinal herb, has potent antiaggregation effects on Alzheimer's beta-amyloid proteins. *J. Neurosci. Res.* **84**, 427–433.

Hofmann T., Glabasnia A., Schwarz B. *et al.* (2006) Protein binding and astringent taste of a polymeric procyanidin, 1,2,3,4,6-penta-*O*-galloyl-beta-D-glucopyranose, castalagin, and grandinin. *J. Agric. Food. Chem.* **54**, 9503–9509.

Hsieh C. L., Cheng C. Y. and Tsai T. H. (2006) Paeonol reduced cerebral infarction involving the superoxide anion and microglia activation in ischemia-reperfusion injured rats. *J. Ethnopharmacol.* **106**, 208–215.

Iwasaki K., Kobayashi S., Chimura Y. *et al.* (2004) A randomized, double-blind, placebo-controlled clinical trial of the Chinese medicinal herb "ba wei di huang wan" in the treatment of dementia. *J. Am. Geriatr. Soc.* **52**, 1518–1521.

Iwasaki K., Satoh-Nakagawa T., Maruyama M. *et al.* (2005) A randomized, observer-blind, controlled trial of the traditional Chinese medicine Yi-Gan San for improvement of behavioral and psychological symptoms and activities of daily living in dementia patients. *J. Clin. Psychiatry* **66**, 248–252.

Kirkitadze M. D., Bitan G. and Teplow D. B. (2002) Paradigm shifts in Alzheimer's disease and other neurodegenerative disorders: the emerging role of oligomeric assemblies. *J. Neurosci. Res.* **69**, 567–577.

Le Bars P. L., Katz M. M., Berman N. *et al.* (1997) A placebo-controlled, double-blind, randomized trial of an extract of Ginkgo biloba for dementia. North American EGb Study Group. *JAMA* **278**, 1327–1332.

Li Y., Kim J., Li J. *et al.* (2005) Natural anti-diabetic compound 1,2,3,4,6-penta-*O*-galloyl-D-glucopyranose binds to insulin receptor and activates insulin-mediated glucose transport signaling pathway. *Biochem. Biophys. Res. Commun.* **336**, 430–437.

Lin H. C., Ding H. Y., Ko F. N. *et al.* (1999) Aggregation inhibitory activity of minor acetophenones from *Paeonia* species. *Planta Med.* **65**, 595–599.

Millard C. B. and Broomfield C. A. (1995) Anticholinesterases: medical applications of neurochemical principles. *J. Neurochem.* **64**, 1909–1918.

Nakagawasai O., Yamadera F., Iwasaki K. *et al.* (2004) Effect of kami-untan-to on the impairment of learning and memory induced by thiamine-deficient feeding in mice. *Neuroscience* **125**, 233–241.

Ono K., Hasegawa K., Naiki H. *et al.* (2004) Curcumin has potent anti-amyloidogenic effects for Alzheimer's beta-amyloid fibrils in vitro. *J. Neurosci. Res.* **75**, 742–750.

Park C. H., Lee Y. J., Lee S. H. *et al.* (2000) Dehydroevodiamine HCl prevents impairment of learning and memory and neuronal loss in rat models of cognitive disturbance. *J. Neurochem.* **74**, 244–253.

Rivière C., Richard T., Vitrac X. *et al.* (2008) New polyphenols active on beta-amyloid aggregation. *Bioorg. Med. Chem. Lett.* **18**, 828–831.

Selkoe D. J. (2002) Alzheimer's disease is a synaptic failure. *Science* **298**, 789–791.

Suemoto T., Okamura N., Shiomitsu T. *et al.* (2004) *In vivo* labeling of amyloid with BF-108. *Neurosci. Res.* **48**, 65–74.

Suzuki T., Arai H., Iwasaki K. *et al.* (2001) A Japanese herbal medicine (Kami-Untan-To) in the treatment of Alzheimer's disease: A pilot study. *Alzheimer's Rep.* **4**, 177–182.

Tierney M. C., Fisher R. H., Lewis A. J. *et al.* (1988) The NINCDS-ADRDA Work Group criteria for the clinical diagnosis of probable Alzheimer's disease: a clinicopathologic study of 57 cases. *Neurology* **38**, 346–359.

Wirths O., Multhaup G. and Bayer T. A. (2004) A modified β-amyloid hypothesis: intraneuronal accumulation of the β-amyloid peptide – the first step of a fatal cascade. *J. Neurochem.* **91**, 513–520.

Yang F., Lim G. P., Begum A. N. *et al.* (2005) Curcumin inhibits formation of amyloid beta oligomers and fibrils, binds plaques, and reduces amyloid in vivo. *J. Biol. Chem.* **280**, 5892–5901.

Yasuda T., Kon R., Nakazawa T. *et al.* (1999) Metabolism of Paeonol in rats. *J. Nat. Prod.* **62**, 1142–1144.

 J. Neurochem. (2009) **109**, 1648–1657

Expert Opinion

Advances in molecular imaging for the diagnosis of dementia

Nobuyuki Okamura, Michelle T Fodero-Tavoletti, Yukitsuka Kudo, Christopher C Rowe, Shozo Furumoto, Hiroyuki Arai, Colin L Masters, Kazuhiko Yanai & Victor L Villemagne†

†*Center for PET, Austin Health, Nuclear Medicine, Melbourne, Australia*

Background: There is an urgent need for early diagnosis and treatment of dementia to ease caregiver burden and medical costs associated with the increasing number of affected patients. Molecular imaging with target-specific ligands is contributing to the early diagnosis of dementia and the evaluation of anti-dementia therapy. *Objective*: This article reviews recent advances in the molecular imaging field applied to dementia. To illustrate the utility of molecular imaging in the clinical management of dementia, results from recently published papers using new imaging probes are compared with those from conventional imaging strategies. *Conclusion*: The recent development of β-sheet binding agents including FDDNP, PIB, SB-13, BF-227 and BAY94-9172 enables the non-invasive detection of amyloid deposition in the brain. These agents would be useful for the early and accurate diagnosis of Alzheimer's disease, patient selection for disease-modifying therapeutic trials and monitoring the effect of anti-amyloid therapy. Also, monitoring neurotransmitter function contributes to the differential diagnosis of dementia and refinement of treatment protocols. New targets for molecular imaging are focusing on protein misfolding diseases associated with the neurotoxic deposition of aggregated tau, α-synuclein and prion proteins.

Keywords: acetylcholine, Alzheimer's disease, amyloid-β protein, dementia, imaging, molecular imaging, near-infrared, positron emission tomography, prion, single photon emission computed tomography, tau

Expert Opin. Med. Diagn. (2009) 3(6):705-716

1. Introduction

Dementia is a common and life-threatening disease in elderly people. The prevalence of dementia increases after the age of 65, resulting in an increasing medical and socio-economic burden. Alzheimer's disease (AD) is the most common cause of dementia and currently affects 4 million people in the US. AD generally begins insidiously with mild memory problems and progresses to the development of functional impairment in multiple cognitive domains within a few years. Elderly people usually complain of increasing forgetfulness with age. However, not all subjects with mild memory impairments progress to dementia. It is important to develop diagnostic methods that have adequate sensitivity and specificity to distinguish those who are likely to develop AD from those memory-impaired individuals who do not. In addition, it is important to predict accurately who might be at an increased risk for AD from a large pool of elderly people. The arrival of new therapies that may delay disease progression emphasizes the need to improve the diagnostic certainty early in the course of AD.

Structural neuroimaging techniques, such as computed tomography (CT) and magnetic resonance imaging (MRI), are routinely used in the screening of cerebrovascular and space-occupying lesions, in the differential diagnosis of normal-pressure hydrocephalus and AD, and in the evaluation of brain atrophy. Widespread cortical

informa
healthcare

10.1517/17530050903133790 © 2009 Informa UK Ltd ISSN 1753-0059

atrophy, a thinning of the medial temporal lobe structures and white matter hyperintensities are, although not pathognomonic, consistent structural neuroimaging findings associated with the progression of AD, where there is a significant overlap with the normal ageing process and with other pathological conditions. Modern molecular neuroimaging techniques such as positron emission tomography (PET) and single photon emission computed tomography (SPECT) have helped in the differential diagnosis of dementia while also allowing the exploration of specific molecular mechanisms of AD.

The pathological hallmarks of AD are the deposition of senile plaques (SPs) and neurofibrillary tangles (NFTs). Whereas NFTs are intraneuronal bundles of paired helical filaments mainly composed of the aggregates of an abnormally phosphorylated form of tau protein, senile plaques consist of extracellular aggregates of amyloid β-peptide (Aβ). Dementia with Lewy bodies (DLB) represents the second most frequent cause of neurodegenerative dementia in the elderly. Insoluble aggregates of α-synuclein called Lewy bodies are the pathological hallmarks of DLB as well as Parkinson's disease (PD), however Lewy bodies are found not only in PD and DLB, but also in AD and other neurodegenerative conditions. Furthermore, neocortical Aβ burden is frequently observed in DLB patients, indicating substantial overlap in the pathology of AD and DLB. To understand precisely the molecular mechanisms of dementia, it is thus important to identify the contribution of each of these pathologies to the dementia syndrome.

2. Cerebral glucose metabolism and cerebral blood flow

Molecular neuroimaging using PET and SPECT has been widely used for the early and differential diagnosis of dementia. Regional hypoperfusion and hypometabolism in the posterior cingulate and temporoparietal cortices is one of the earliest changes in AD and is a prognostic marker in subjects with mild cognitive impairment (MCI) [1]. The development of voxel-by-voxel analysis techniques has made substantial contributions to the early identification of these regional brain changes [2]. A comparison study of fluoro-deoxy glucose (FDG)-PET and perfusion SPECT indicated that FDG-PET is more sensitive than SPECT because the magnitude of the hypometabolism observed with FDG-PET is generally greater than the degree of the hypoperfusion seen with SPECT [3]. FDG-PET is a sensitive technique for the early identification of AD patients where hypometabolism has been observed even in cognitively normal individuals who have a higher genetic risk of developing AD [4]. In a multi-center study, the prognostic value of FDG-PET showed a high degree of sensitivity (93%) in the evaluation of dementia [5]. However, the specificity (73%) is not completely at a satisfactory level for the prediction of progressive dementia.

Another important application of FDG-PET lies in the differential diagnosis of AD from other causes of dementia, such as DLB and frontotemporal dementia (FTD). The consortium on dementia with Lewy bodies (CDLB) characterized DLB as a progressive cognitive decline, extrapyramidal symptoms, episodic confusion, hallucinations and fluctuating cognitive impairment [6]. However, several follow-up studies indicated that although the CDLB criteria present an appropriate specificity, it is laden with a relatively poor sensitivity [7]. In addition, differential diagnosis of DLB from AD is difficult even in the later stages of the disease. DLB differs from AD in the treatment response experienced by patients. For example, DLB patients are at high risk for severe reactions to antipsychotic drugs. This highlights a need to develop a sensitive diagnostic tool to provide greater precision in the antemortem diagnosis of DLB. Clinical PET and SPECT studies showed a characteristic pattern of regional glucose hypometabolism and hypoperfusion in the primary visual cortex and the occipital association cortex in addition to the temporoparietal pattern of abnormal cerebral blood flow and metabolism found in AD [8].

The ideal biomarker for AD should have a diagnostic sensitivity > 80% for detecting AD and a specificity of > 80% for distinguishing other dementias. Hanyu *et al.* indicated that a diagnostic strategy combining perfusion SPECT and mini mental state examination (MMSE) performance has produced a sensitivity of 81% and a specificity of 85% in the differentiation of DLB from AD [9], which indicates that perfusion SPECT is an ideal diagnostic marker for DLB. PET measures of glucose hypometabolism and SPECT measures of hypoperfusion in the occipital cortex could help to enhance the clinical diagnosis of DLB, particularly in the early stages of the disease, allowing the maximum therapeutic benefit in the treatment of DLB patients. A recent multi-center study demonstrated the usefulness of FDG-PET in the differential diagnosis of AD, DLB and FTD [10]. Differential diagnosis of AD and FTD is a particularly good application for FDG-PET because of the sharp contrast in their pattern of glucose hypometabolism. The addition of FDG-PET to clinical information increased the diagnostic accuracy and confidence for both AD and FTD [11]. In the US, the Center for Medicare and Medicaid Services has recently approved the use of FDG-PET for differential diagnosis of AD from FTD.

3. Imaging neurotransmitter, neuroreceptor and neuroenzymatic function

The evaluation of neurotransmitter functions in the brain is helpful for the determination and monitoring of treatment protocols, prediction of disease progression, as well as for the early diagnosis of dementia. Many radiotracers have been developed for the assessment of neurotransmitter functions, including dopamine, acetylcholine (ACh), serotonin, histamine, benzodiazepine, adenosine, NK-1 and opioid (Table 1) [12]. Some of them have been applied for the assessment of the neurotransmitter changes in dementia [13,14].

Table 1. Radiopharmaceuticals for brain positron emission tomography imaging.

Functions	Drugs
Blood flow	^{15}O-H_2O
Blood volume	^{15}O-CO
Glucose metabolism	^{18}F-FDG
Oxygen metabolism	^{15}O-O_2
Hypoxia	^{18}F-fluoromisonidazole
Amino acid metabolism	^{11}C-methionine
Neurotransmitter	
Dopamine D_1 receptor	^{11}C-SCH23390, ^{11}C-NNC112
Dopamine D_2 receptor	^{11}C-raclopride, ^{11}C-methylspiperone, ^{11}C-nemonapride, ^{11}C-FLB457
Dopamine transporter	^{11}C-β-CIT, ^{11}C-CFT, ^{11}C-cocaine, ^{11}C-methylphenidate, ^{11}C-PE2I
Dopamine synthesis	^{11}C-DOPA, ^{18}F-DOPA
Muscarinic acetylcholine receptor	^{11}C-NMPB, ^{11}C-TRB, ^{18}F-FP-TZTP
Nicotinic acetylcholine receptor	^{11}C-nicotine, ^{18}F-norchloro-fluoro-homoepibatidine, ^{18}F-fluoro-A-85380
Acetylcholine esterase	^{11}C-MP4A, ^{11}C-PMP, ^{11}C-physostigmine, ^{11}C-donepezil
Serotonin 5-HT_{1A} receptor	^{11}C-WAY100635, ^{18}F-FCWAY
Serotonin 5-HT_{2A} receptor	^{11}C-methylspiperone, ^{11}C-MDL 100907, ^{18}F-altenserin, ^{18}F-setoperone
Histamine H_1 receptor	^{11}C-doxepin, ^{11}C-pyrilamine
Central benzodiazepine receptor	^{11}C-flumazenil, ^{18}F-flumazenil
Peripheral benzodiazepine receptor	^{11}C-PK11195, ^{11}C-FEDAA1106, ^{11}C-PBR28, ^{11}C-DPA-713, ^{11}C-CLINME
Adenosine receptor	^{11}C-MPDX, ^{11}C-TMSX
NK-1 receptor	^{11}C-CP-99994, ^{18}F-SPA-RQ
Opioid receptor	^{11}C-carfentanyl, ^{11}C-diprenorphine, ^{18}F-cyclofoxy
Protein aggregate	
Amyloid β protein	^{11}C-PIB, ^{11}C-SB13, ^{11}C-BF227, ^{18}F-FDDNP, ^{18}F-BAY94-9172

One of the major alterations found in the brains of AD patients is a loss of neurons in the cholinergic nucleus basalis of Meynert [15]. A loss of the cholinergic markers cholineacetyltransferase (ChAT) and acetylcholinesterase (AChE) is observed in post-mortem AD brains [16]. In addition, a loss of the cholinergic function is closely related with the severity of cognitive impairment in dementia [17]. Therefore, the cholinergic hypothesis has served as the basis for treatment in AD [18], and attempts to treat the cognitive dysfunction in AD have been focused on enhancing the cholinergic function through AChE inhibitors [19]. AChE inhibitors in AD therapy should boost endogenous levels of ACh in the brain and thereby enhance the cholinergic neurotransmission. Several AChE inhibitors are now used for the symptomatic treatment of AD. Functional imaging of cholinergic neurotransmission is a useful strategy for the determination of the treatment protocol of demented patients. The use of tracers that are hydrolyzed specifically by AChE permits the measurement and imaging of local AChE activity in humans [20]. Clinical PET studies using [^{11}C]MP4A and [^{11}C]PMP indicated that AChE activity is prominently reduced in AD [21,22]. A recent [^{11}C]MP4A PET study demonstrated further significant reduction of AChE activity in the medial occipital cortex of PD and DLB patients [23]. The reduction of cortical k_3 value was greater in DLB patients (27.1%) than AD patients (13%), suggesting it might be useful in differentiating AD from DLB. The second approach to the evaluation of AChE function is using the AChE inhibitors themselves as radiotracers. This method enables a direct investigation of the pharmacokinetics of AChE inhibitors using PET. Donepezil hydrochloride is at present the AChE inhibitor most widely used for the treatment of AD and shows a selective binding of AChE compared with butyrylcholinesterase [24]. Radiolabeled donepezil can thus be used as a tracer to measure the concentration of brain AChE *in vivo*. A [^{11}C]donepezil PET study clearly revealed higher concentrations of tracer distribution in the striatum and cerebellum than in the neocortex and a prominent reduction of donepezil binding in the brains of AD patients [25]. The correlation of donepezil binding with severity of dementia was observed with AD patients. The amount of therapeutic drug bound to AChE is considered to be a key factor in determining the treatment response in each patient. A post-treatment PET study following the administration of 5 mg donepezil a day revealed an ~ 60% reduction of [^{11}C]donepezil binding throughout the brain [25]. This finding indicates that the AChE occupancy by orally administered donepezil was ~ 40% in daily doses of 5 mg. A [^{11}C]MP4A PET study revealed a mean 39% reduction in AChE activity after oral administration of 3 – 5 mg donepezil [26]. These findings together suggest that inhibition of AChE activity matches occupancy of AChE inhibitor binding sites. The *in vivo* evaluation of AChE occupancy using [^{11}C]donepezil PET could thus be a powerful strategy for determining the optimal dose of donepezil in AD therapy. Nicotinic ACh receptors have also been implicated in a variety of central processes, such as memory and cognition [27,28]. Abnormally low densities of nicotinic ACh receptors have been measured *in vitro* in autopsy brain tissue of AD patients [29]. Only PET studies using [^{11}C]nicotine found reduced uptake and binding in the temporal and frontal cortices of AD patients [28]. However, a recent PET study using 2-[^{18}F]fluoro-A-85380 found no evidence of *in vivo* nicotinic ACh receptor loss in early AD despite significant cognitive impairment [30]. Although the main focus of

neuroceptor studies in AD has been the study of nicotinic ACh receptors, muscarinic ACh receptors, especially the M1 and M2 muscarinic ACh receptors subtypes, have also been implicated in AD [31]. Highly selective subtype-specific radioligands for M1 or M2 muscarinic ACh receptors are not yet available [32], but radiotracers that can assist in both quantifying muscarinic ACh receptor densities and monitoring AD therapy are being developed [33].

One of the major neuropathological findings in DLB is the loss of dopaminergic neurons in the substantia nigra. Such neuronal loss can be quantified by assessing striatal dopaminergic terminals with PET or SPECT, using ligands specific for the dopamine transporter, such as [^{123}I]-β-CIT and [^{123}I]FPCIT [34,35]. The evaluation of presynaptic dopamine synthesis by [^{18}F]FDOPA PET demonstrated a prominent reduction in striatal accumulation in DLB patients [36], while the assessment of striatal dopaminergic terminals with vesicular monoaminergic transporter type 2 (VMAT2) tracers is also useful in distinguishing AD from DLB [37], suggesting that the assessment of the nigrostriatal dopaminergic function using PET and SPECT would be an informative diagnostic adjunct in distinguishing DLB from other types of neurodegenerative dementia. Another strategy to gain an accurate differential diagnosis of DLB from AD is the assessment of the cardiovascular autonomic dysfunction using scintigraphy with [^{123}I]metaiodobenzylguanidine (MIBG). This tracer enables the quantification of the post-ganglionic cardiac sympathetic innervation. Several studies using [^{123}I] MIBG scintigraphy have demonstrated a reduced cardiac retention compared with mediastinal uptake in DLB, as opposed to AD [38,39].

4. Imaging of neuroinflammation

Microglia are the primary resident immune surveillance cells in the brain and are thought to play a significant role in the pathogenesis of several neurodegenerative disorders, including AD [40]. *In vivo* measurement of microglial activation may help chart the progression of neuroinflammation as well as assess the efficacy of therapies designed to modulate neuroinflammation. Activated microglia can be measured using radioligands for the peripheral benzodiazepine receptor. [^{11}C]PK11195 has been widely used for this purpose in several neurodegenerative disorders. A recent PET study using [^{11}C]PK11195 demonstrated significant increase in microglial activation in AD brains and correlation of cortical microglial activation with the severity of dementia, which is compatible with a role of microglia in neuronal damage [41,42]. However, recent PET studies also indicated that cortical microglial activation measured by [^{11}C]PK11195 is not associated with amyloid deposition in the early stage of AD [43,44]. Despite its wide application, [^{11}C]PK11195 has a high lipophilicity and a high nonspecific binding, which makes it difficult to perform an accurate and sensitive measurement of microglial activation. Therefore, efforts are being made to develop more sensitive radiotracers for the peripheral benzodiazepine receptor [45].

5. Imaging amyloid deposits in the brain

As mentioned before, the pathological hallmarks of AD are SPs and NFTs [46]. SPs are composed of amyloid-β (Aβ) protein. Aβ is a 4 kDa 39 – 43 amino acid metalloprotein derived from the proteolytic cleavage of the amyloid precursor protein (APP) by β- and γ-secretases. The abnormal accumulation of SPs has been implicated as the central event in the etiology and pathogenesis of AD [47] and precedes the cognitive decline observed in AD [48]. *In vivo* detection of SPs in the brain enables the identification of AD pathology even in subjects in their presymptomatic stage. A deeper understanding of the molecular mechanism of Aβ formation, degradation and neurotoxicity is being translated into new therapeutic approaches. The most promising approaches focus on reducing Aβ formation through β- and γ-secretase inhibitors or on increasing the removal of Aβ by immunotherapy or metal–protein attenuating compounds aimed at blocking the formation of Aβ oligomers and fibrils, inhibiting neurotoxicity [49,50]. For the assessment of preventive intervention and monitoring of therapeutic effects, it is desirable to measure non-invasively the amount of Aβ deposit in the living brain.

Although these Aβ deposits are still well beyond the resolution of conventional neuroimaging techniques, the density of these deposits in the brain tissue can be measured through specific radiotracer and nuclear medicine techniques. Many β-sheet binding agents have been developed as Aβ binding radiotracers for PET and SPECT imaging. The chemical structures of PET amyloid imaging agents are shown in **Figure 1**. The first compound to emerge as an amyloid-imaging agent was Chrysamine-G [51]. This compound shows similar binding characteristics as Congo Red but, unfortunately, its blood–brain barrier (BBB) permeability of Chrysamine-G is limited. Other derivatives including 1-bromo-2,5-bis-(3-hydroxycarbonyl-4-hydroxy) styrylbenzene (BSB), 1-iodo-2,5-bis-(3-hydroxycarbonyl-4-hydroxy) styrylbenzene (ISB), X-34 and methoxy X-04 have also been developed to improve BBB permeability [52-55]. Among them, BSB successfully visualized the brain amyloid deposits of APP transgenic mice after the intravenous administration of this compound. However, the BBB permeability of this agent was still inadequate to use as a clinical PET tracer. A marked progression in the development of amyloid-imaging tracers was the development of 2-(1-{6-[(2-[^{18}F]fluoroethyl)(methyl)amino]-2-naphthyl} ethylidene)malononitrile([^{18}F]FDDNP) [56,57]. This compound is highly lipophilic and can easily cross the BBB, and has been used in human PET studies. The [^{18}F]FDDNP PET scan successfully differentiated people with AD and MCI from those with no cognitive impairment [58]. This agent has some limitations in its practical use owing to its low signal-to-background ratio. Direct comparison of [^{18}F]

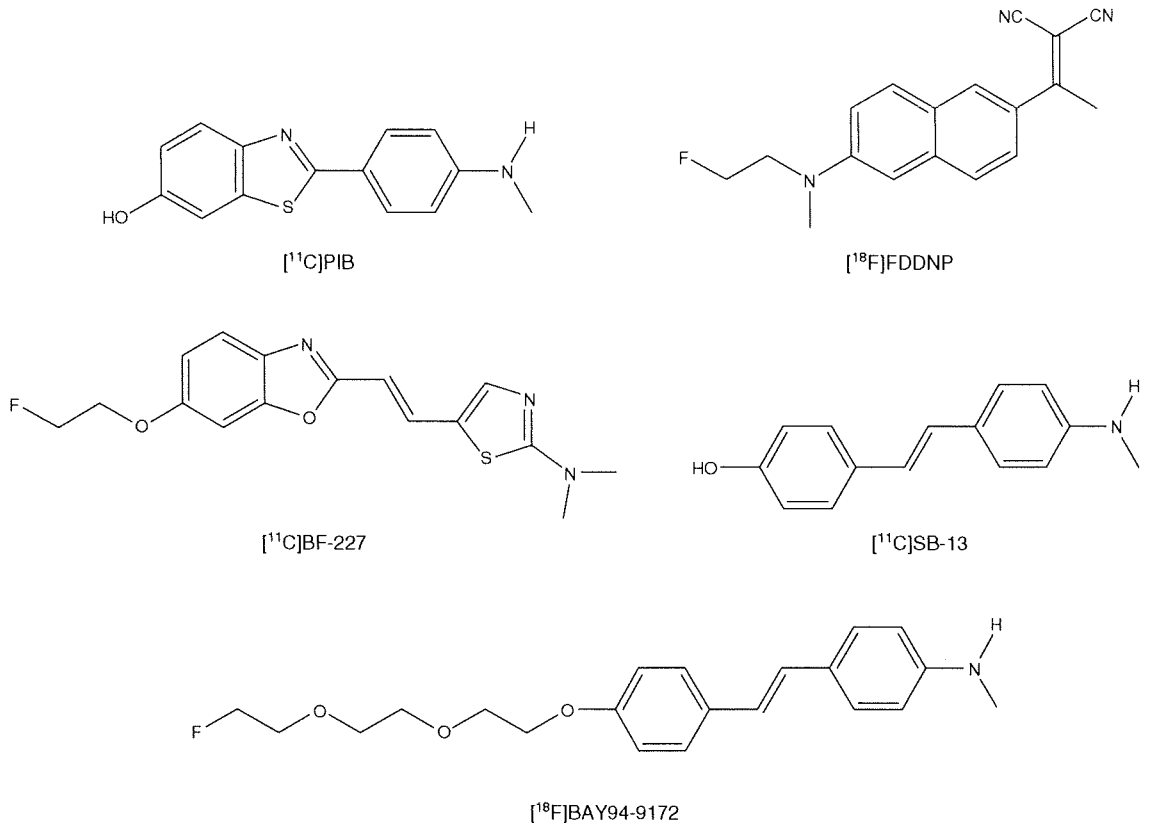

Figure 1. Chemical structures of β-sheet binding agents.

FDDNP PET and [^{11}C]PIB PET showed lower specific binding of [^{18}F]FDDNP in AD patients than that of [^{11}C]PIB [59]. However, marked differences in tracer distribution were observed between these tracers. Intriguingly, negligible PIB but strong FDDNP binding was in the medial temporal cortex of AD patients, suggesting higher binding affinity of FDDNP to NFTs than PIB [60].

At present, the most successful amyloid-binding agent is a thioflavin-T derivative, *N*-methyl-[^{11}C] 2-(4′-methylaminophenyl)-6-hydroxybenzothiazol ([^{11}C]PIB), which has been shown to possess a high affinity for Aβ fibrils [61,62]. An autoradiographic study using AD brain sections revealed that [^{11}C] PIB, in addition to binding to the classical fibrillar Aβ plaques, also binds to a range of Aβ-containing lesions, including diffuse plaques and cerebrovascular amyloid angiopathy [63]. Micro-PET evaluations in transgenic mice models of AD were performed with a high specific activity [^{11}C]PIB, showing [^{11}C]PIB retention colocalizing with plaques [64]. It was also reported that PIB preferentially binds one kind of the N-terminal truncated Aβ1-42(43) species in senile plaques, more specifically, the one truncated at position three (Aβ3(pE)), displaying a fivefold higher affinity for Aβ3(pE)1-42(43) than for Aβ1-42(43). This is relevant because the accelerated formation of plaques seems to be associated with this Aβ3(pE)1-42(43) species [65]. *In vitro* binding studies indicated that PIB preferentially binds to Aβ1-42 fibrils with high affinity [61]. Positive PIB staining of DLB brain sections colocalized with immunoreactive Aβ plaques, but failed to stain Lewy bodies, whereas image quantification analysis suggested that given the small size and low density of Lewy bodies within the brains of DLB subjects, any contribution of Lewy bodies to the [^{11}C] PIB PET signal would be negligible [66]. In a similar way as with α-synuclein fibrils, PIB binds to NFTs with a comparatively lower affinity than Aβ [63], further confirming that the *in vivo* PIB cortical uptake primarily reflects Aβ-related cerebral amyloidosis.

[^{11}C]PIB retention can be quantified through binding potential (BP), distribution volume ratios (DVR) or, semi-quantitatively, through standardized uptake value ratios (SUVR). DVR can be calculated through Logan graphical analysis of dynamic PET data and either using metabolite-corrected arterial plasma as input function or the radioactivity in the cerebellar cortex – a region generally devoid of SPs – as a reference region. Quantitative assessment of PIB retention was validated by studies performed in controls, MCI and AD patients [67,68]. These studies showed that DVR of PIB in AD patients was nearly twice that in controls in the neocortex.

The quantitative DVR measurement based on arterial input function is generally considered as the gold standard; however, the semiquantitative SUVR method without arterial blood sampling is widely used as a simple approach to estimate Aβ burden. Comparison of several quantitative and semiquantitative methods showed that the SUVR approach was the most robust in terms of test–retest variability and maximum effect size between AD patients and controls [68]. However, disadvantages of the SUVR include inherent bias and potential for time-varying outcomes. A recent report selected the 50 – 70 min post-injection time window for SUVR measurement in PIB-PET as the best compromise between physiologic validity, agreement of outcomes and study feasibility [69]. Cerebral atrophy can cause underestimation of PET measurements. Thus, the failure to account for the effect of partial-volume effects in brains with expanded sulci has contributed to the confounding results in functional imaging studies of ageing and dementia [70]. A recent study indicated that partial volume correction led to a small positive bias, but did not affect discriminatory performance between AD patients and controls [71]. However, partial volume correction is paramount in the analysis of patients with severe cerebral atrophy.

[^{11}C]PIB PET studies in human subjects have shown a robust difference between the retention pattern in AD patients and healthy controls, with AD cases showing a significantly higher retention of [^{11}C]PIB in the neocortical areas of the brain affected by Aβ deposition [72,73]. The [^{11}C]PIB retention in the neocortical areas is correlated with the Aβ plaque load (**Figure 2**) [74-76]. Most of frontotemporal dementia cases show no increase in PIB retention. By contrast, ~ 80% of DLB cases showed abnormal PIB DVR values in the neocortex [73]. [^{11}C]PIB DVR values in the neocortex are also higher in DLB patients than in cases of PD with dementia (PDD) [77]. The differential amyloid load of DLB and PDD suggests that these clinically similar conditions can be differentiated on the basis of amyloid deposition. The uptake of [^{11}C]PIB in the brain is also elevated in subjects diagnosed with cerebrovascular amyloid angiopathy and shows a similar distribution as in AD cases [78]. [^{11}C] PIB binding in the brain is correlated with the rate of cerebral atrophy in AD subjects [79], and with decreased cerebrospinal fluid (CSF) Aβ1-42 in both demented and non-demented subjects [80]. Multimodality studies in early AD patients have shown that the Aβ deposition correlates with atrophy and metabolism reduction in posterior cortical regions [81]. Also, this deposition is inversely correlated with the activation of language centers, leading to a functional reorganization of the language system [82]. Intriguingly, ~ 30% of the healthy control subjects showed a cortical binding of [^{11}C] PIB, predominantly in the prefrontal cortex and the posterior cingulate/precuneus areas, with some of them displaying the same degree of retention as observed in AD subjects [73,83,84]. Approximately 20 – 30% of healthy, age-matched subjects showed elevated BP values, predominantly in the prefrontal and posterior cingulate cortices [73,83]. The demonstration of [^{11}C]PIB binding in a proportion of elderly normal subjects supports the post-mortem observation that the Aβ aggregation occurs predominantly before the onset of dementia [48]. However, there is at present no evidence of how many PIB-positive normal individuals will develop dementia or how long the interval is between the detection of significant Aβ burdens and the onset of dementia. Longitudinal studies are needed to elucidate the relation between amyloid deposition and time course of AD.

Amnestic MCI is considered a prodromal state of AD, though not all individuals with MCI will develop AD; MCI converters and non-converters are difficult to distinguish prospectively from a clinical and neuropsychological perspective. Analysis of PIB-PET images in MCI subjects revealed a bimodal distribution of PIB retention in the neocortex. About two-thirds of MCI cases showed neocortical PIB retention similar in distribution (and sometimes in degree) to AD, whereas the other third of MCI cases showed no cortical retention, similar to healthy elderly individuals [73,85,86]. A recent study demonstrated higher PIB retention in MCI converters than in non-converters, suggesting the utility of amyloid imaging in the prediction of progression to dementia [86]. Comparison of FDG-PET and PIB-PET demonstrated better group discrimination in non-amnestic and amnestic MCI subjects by PIB-PET [71]. A direct comparison of MRI with PIB-PET was also performed in the control, MCI and AD populations [87]. The voxel-by-voxel comparisons of AD versus control patients revealed differences in the topographical distribution of amyloid deposition and in grey matter loss, suggesting that these two imaging strategies provide complementary information about AD pathology.

Longitudinal assessment of PIB retention is potentially useful for the assessment of treatment efficacy of anti-amyloid therapies. Two serial PIB-PET studies demonstrated that AD patients showing cognitive decline and deterioration of cerebral glucose metabolism were stable in neocortical PIB retention over 2 years and an overall change in neocortical PIB retention of AD patients was below the test–retest reproducibility (3 – 7%) for PIB-PET [88,89]. Jack *et al.* recently demonstrated the dissociation between PIB rate of change and annual change in brain atrophy as measured by MRI [90]. They demonstrated that PIB retention proceeds at a constant slow rate whereas the atrophy rate in MRI accelerates during the course of AD. In addition, clinical symptoms of AD were closely associated with the rate of atrophy as measured by MRI, but not to the rate of Aβ deposition as measured by PIB-PET. From these results, it can be speculated that amyloid deposition reaches a plateau before the presentation of dementia and its slow increase does follow a parallel course with the clinical progression of AD.

Although SPECT studies with ^{123}I-labeled 6-iodo-2-(49-dimethylamino-) phenyl-imidazo[1,2-α]pyridine (IMPY) and its derivatives have not yet fulfilled their potential as amyloid-imaging probes [91], other promising candidates for amyloid-imaging agents can be found among stilbene and

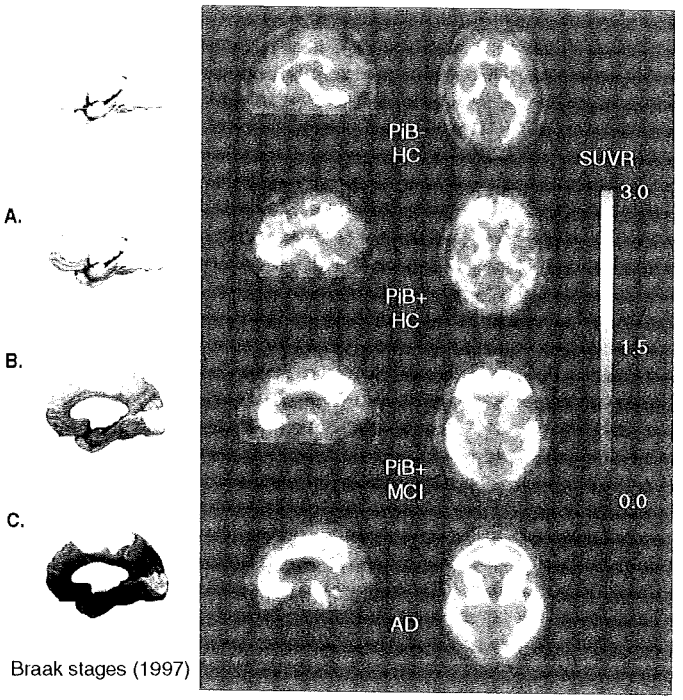

Figure 2. Representative sagittal and transaxial positron emission tomography images showing the different regional uptake of [^{11}C]PIB in two asymptomatic healthy age-matched controls (PiB-negative HC and PiB-positive HC), a participant with mild cognitive impairment (MCI) and a participant with Alzheimer's disease (AD) (right), along with schematics showing the stages of Aβ deposition in the human brain as proposed by Braak and Braak (1997) (left).

Braak, H., & Braak, E. (1997). Frequency of stages of Alzheimer-related lesions in different age categories. Neurobiology of Aging, 18(4), 351-357.

AD: Alzheimer's disease; SUVR: Standardized uptake value ratios.

styrylpyridine derivatives [92]. In an early clinical study, the ^{11}C-labeled stilbene derivative 4-*N*-methylamino-4′-hydroxystilbene (SB-13) demonstrated an abnormal tracer uptake in the AD brain [93]. Benzoxazole derivatives are also promising alternatives for amyloid-imaging probes [94]. A PET study using the ^{11}C-labeled benzoxazole derivative 2-(2-[2-dimethylaminothiazol-5-yl]ethenyl)-6-(2-[fluoro]ethoxy) benzoxazole (BF-227) demonstrated the retention of this tracer in cerebral cortices of AD patients, but not in those of healthy elderly subjects. AD patients were clearly distinguishable from healthy elderly individuals using neocortical uptake of [^{11}C]BF-227 [95]. A voxel-by-voxel analysis demonstrated a higher retention of [^{11}C]BF-227 in the posterior association cortex of AD patients. The pattern of this distribution corresponds well with the distribution of neuritic plaque depositions in post-mortem AD brains. These findings suggest that [^{11}C]BF-227 is a promising PET probe for *in vivo* detection of dense amyloid deposits in AD patients.

Owing to the limited half-life of ^{11}C (20.4 min), the use of ^{11}C-labeled agents is limited to facilities with an on-site cyclotron. ^{18}F has a much longer radioactive half-life (109.7 min) than ^{11}C, allowing Aβ imaging at PET centers without on-site cyclotrons. There are two major difficulties in developing ^{18}F-labeled PET agents: fluorination increases lipophilicity, resulting in slower clearance from myelin-rich brain structures such as white matter, and incorrect labeling with ^{18}F sometimes leads to defluorination and ^{18}F accumulation in bone. A recent PET study using the ^{18}F-labeled stilbene derivative *trans*-4-(N-methylamino)-4′-{2-[2-(2-[^{18}F]fluoro-ethoxy)-ethoxy]-ethoxy}-stilbene (BAY94-9172) showed widespread neocortical retention in AD patients [96]. The binding of [^{18}F]BAY94-9172 matched the histopathological distribution of amyloid plaques in AD and clearly discriminated between AD and healthy controls. This tracer provides images of similar appearance to [^{11}C]PIB PET without the inherent limitation of the 20 min half-life.

6. Expert opinion

AD and many other neurodegenerative disorders, including FTD, progressive supranuclear palsy, corticobasal degeneration, PD, DLB, multiple system atrophy and prion disease, belong to the family of protein misfolding diseases, characterized by protein self-aggregation and deposition (**Table 2**). The tissue deposits observed in the brains of these diseases usually contain an enriched β-sheet structure, suggesting a potential target for

Table 2. Protein misfolding diseases and their fibrillar deposits.

Protein	Fibrillar deposits	Diseases
Amyloid β	Senile plaque Cerebrovascular amyloid	Alzheimer's disease Down's syndrome Cerebral amyloid angiopathy
Tau	Neurofibrillary tangle Pick body Tufted astrocytes Astrocytic plaque	Alzheimer's disease Frontotemporal lobar degeneration Progressive supranuclear palsy Corticobasal degeneration
α-Synuclein	Lewy body Glial cytoplasmic inclusions	Parkinson's disease Dementia with Lewy bodies Multiple system atrophy
Prion	Prion plaque	Creutzfeldt–Jakob disease Variant Creutzfeldt–Jakob disease Gerstmann-Sträussler-Scheinker disease
TDP-43	Neuronal cytoplasmic inclusion Neuronal intranuclear inclusion Skein-like inclusion	Frontotemporal lobar degeneration Amyotrophic lateral sclerosis Guam parkinsonism-dementia complex

Table 3. Comparison of positron emission tomography and near-infrared fluorescence imaging.

	PET imaging	Near-infrared fluorescence imaging
Amount of probe required	Low (nanograms per body)	High (micrograms to milligrams per body)
Spatial resolution	High (several millimeters)	Low (depending on the depth of object)
Time resolution	Low (min)	High (sec)
Quantitativity	High (absolute quantitation)	Low (relative quantitation)
Measurable depth range	No limit (whole brain)	Limited (< 10 cm)
Invasiveness	Yes (radiation exposure)	No
Cost of imaging devices	High (several million US$)	Low (tens or hundreds of thousands US$)

non-invasive imaging by β-sheet binding agents. Thus, molecular PET imaging has the potential to be extended to this wide spectrum of protein misfolding diseases. Specifically, an *in vivo* imaging technique for aggregated tau proteins is most needed because NFTs as well as SPs are the major hallmarks in the pathology of AD. Neuropathological studies suggest that the loss of neuronal function and disease severity are more closely correlated to the density of NFTs than to the density of SPs. Furthermore, the deposition of NFTs also starts before the presentation of clinical symptoms in AD [48]. Even in the very early stages of AD, patients display a considerable number of NFTs in the entorhinal cortex and the hippocampus, sufficient for the neuropathological diagnosis of AD. Prevention of NFT formation is thus an important target of anti-dementia drugs. The inhibition of abnormal tau hyperphosphorylation, its aggregation, and the direct stabilization of microtubules appear to be promising therapeutic strategies in AD [95]. Thus, the non-invasive evaluation of tau pathology would not only assist in the early diagnosis of AD and other tauopathies, but also facilitate the monitoring of the efficacy of such new treatments. Although FDDNP-PET is reported to detect both Aβ and tau pathologies in the AD brain [56-58], no surrogate markers are available for selectively evaluating the deposition of NFTs. Selective tau imaging agents for PET and SPECT are still in the development stage [97]. Prion proteins are another target of β-sheet binding agents. Actually, Aβ binding agents have shown a high binding affinity to prion amyloid deposits because these prion deposits share the common secondary β-sheet structure with brain Aβ deposits in the AD. Therefore, existing β-sheet binding agents would be useful for the *in vivo* detection of prion amyloid plaques in the brain. A clinical PET study using FDDNP and PIB in familial Creutzfeldt–Jacob disease (CJD) patients with a PrP gene mutation [98] showed a moderate retention of FDDNP and no retention of PIB in the brain, suggesting that FDDNP has a greater binding affinity for prion amyloid plaques than PIB. Similar lack of PIB retention was reported for two cases of autopsy-confirmed sporadic CJD [99]. For an early and accurate diagnosis of prion disease, agents that can sensitively detect prion amyloid deposits should be explored further.

Near-infrared fluorescence imaging is expected to have a major impact in molecular Aβ imaging, as an alternative to PET. A study using a near-infrared fluorescence oxazine dye, AOI987, has successfully demonstrated the *in vivo* detection of amyloid plaques in the mouse brain using near-infrared fluorescence imaging [100]. For imaging

amyloid in the brain, near-infrared fluorescence probes are required to have a long wavelength (> 600 nm), enough to penetrate the body tissue, and highly selective binding to Aβ. The major limitations of near-infrared fluorescence imaging are the low spatial resolution, the low quantitative ability and the limited measurable depth range (**Table 3**). However, the greatest benefit of near-infrared fluorescence imaging is the relatively lower cost of the imaging devices than in PET imaging. This technique is potentially useful for the screening of amyloid deposition in the population that has a risk of developing dementia.

Molecular imaging is a powerful tool for understanding the pathophysiology of AD. *In vivo* detection of amyloid plaques enables the detection of AD patients in their early stage. Clinical application of tau-specific ligands will contribute towards improved differential diagnosis of dementia and monitoring the severity of tau pathology in the brain. These imaging techniques and forthcoming anti-dementia therapy will contribute to the eradication of AD in the future.

Declaration of interest

This study was partially supported by the Special Coordination Funds for Promoting Science and Technology, the Program for the Promotion of Fundamental Studies in Health Science by the National Institute of Biomedical Innovation, the Industrial Technology Research Grant Program from the New Energy and Industrial Technology Development Organization (NEDO) of Japan, the Health and Labor Sciences Research Grants for Translational Research from the Japanese Ministry of Health, Labor, and Welfare, a JST grant on research and education in molecular imaging, and NHMRC project grant 509166.

Bibliography

1. Minoshima S, Giordani B, Berent S, et al. Metabolic reduction in the posterior cingulate cortex in very early AD. Ann Neurol 1997;42:85-94
2. Matsuda H. Role of neuroimaging in Alzheimer's disease, with emphasis on brain perfusion SPECT. J Nucl Med 2007;48:1289-300
3. Herholz K, Schopphoff H, Schmidt M, et al. Direct comparison of spatially normalized PET and SPECT scans in Alzheimer's disease. J Nucl Med 2002;43:21-6
4. Reiman EM, Caselli RJ, Yun LS, et al. Preclinical evidence of Alzheimer's disease in persons homozygous for the epsilon 4 allele for apolipoprotein E. N Engl J Med 1996;334:752-8
5. Silverman DH, Small GW, Chang CY, et al. Positron emission tomography in evaluation of dementia: regional brain metabolism and long-term outcome. JAMA 2001;286:2120-7
6. McKeith IG, Galasko D, Kosaka K, et al. Consensus guidelines for the clinical and pathologic diagnosis of dementia with Lewy bodies (DLB): report of the consortium on DLB international workshop. Neurology 1996;47:1113-24
7. McKeith I, Mintzer J, Aarsland D, et al. International psychogeriatric association expert meeting on DLB: Dementia with Lewy bodies. Lancet Neurol 2004;3:19-28
8. Donnemiller E, Heilmann J, Wenning GK, et al. Brain perfusion scintigraphy with 99mTc-HMPAO or 99mTc-ECD and 123I-beta-CIT single-photon emission tomography in dementia of the Alzheimer-type and diffuse Lewy body disease. Eur J Nucl Med 1997;24:320-5
9. Hanyu H, Shimizu S, Hirao K, et al. Differentiation of dementia with Lewy bodies from Alzheimer's disease using mini-mental state examination and brain perfusion SPECT. J Neurol Sci 2006;250:97-102
10. Mosconi L, Tsui WH, Herholz K, et al. Multicenter standardized 18F-FDG PET diagnosis of mild cognitive impairment, Alzheimer's disease, and other dementias. J Nucl Med 2008;49:390-8
11. Foster NL, Heidebrink JL, Clark CM, et al. FDG-PET improves accuracy in distinguishing frontotemporal dementia and Alzheimer's disease. Brain 2007;130:2616-35
12. Heiss WD, Herholz K. Brain receptor imaging. J Nucl Med 2006;47:302-12
13. Small GW, Bookheimer SY, Thompson PM, et al. Current and future uses of neuroimaging for cognitively impaired patients. Lancet Neurol 2008;7:161-72
14. Bohnen NI, Frey KA. Imaging of cholinergic and monoaminergic neurochemical changes in neurodegenerative disorders. Mol Imaging Biol 2007;9:243-57
15. Whitehouse PJ, Price DL, Clark AW, et al. Alzheimer disease: evidence for selective loss of cholinergic neurons in the nucleus basalis. Ann Neurol 1981;10:122-6
16. Fishman EB, Siek GC, MacCallum RD, et al. Distribution of the molecular forms of acetylcholinesterase in human brain: alterations in dementia of the Alzheimer type. Ann Neurol 1986;19:246-52
17. Perry EK, Tomlinson BE, Blessed G, et al. Correlation of cholinergic abnormalities with senile plaques and mental test scores in senile. dementia BMJ 1978;25:1457-9
18. Bartus RT, Dean RL, Beer B, et al. The cholinergic hypothesis of geriatric memory dysfunction. Science 1982;30:408-14
19. Giacobini E. Cholinesterases and cholinesterase inhibitors. London: Taylor & Francis Group, 2000
20. Kilbourn MR, Snyder SE, Sherman PS, et al. In vivo studies of acetylcholinesterase activity using a labeled substrate, n-[C-11]methylpiperdin-4-yl propionate ([C-11]PMP). Synapse 1996;22:123-31
21. Iyo M, Namba H, Fukushi K, et al. Measurement of acetylcholinesterase by positron emission tomography in the brains of healthy controls and patients with Alzheimer's disease. Lancet 1997;349:1805-9
22. Kuhl DE, Koeppe RA, Minoshima S, et al. In vivo mapping of cerebral acetylcholinesterase activity in aging and Alzheimer's disease. Neurology 1999;52:691-9
23. Shimada H, Hirano S, Shinotoh H, et al. Mapping of brain acetylcholinesterase alterations in Lewy body disease by PET. Neurology 2009: doi:10.1212/WNL.0b013e3181ab2b58
24. Sugimoto H, Ogura H, Arai Y, et al. Research and development of donepezil hydrochloride, a new type of